An Experimental Investigation of Wave Propagation in Fractured Brittle Material

Thesis by

Bibhuti Bhusan Patel

In Partial Fulfillment of the Requirements

For the Degree of

Aeronautical Engineering

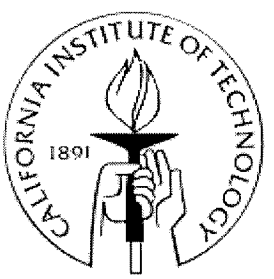

California Institute of Technology

Pasadena, California

1998

(Submitted November 14, 1997)

To my parents,
my sister Rosy
and my brother Bapi.

ACKNOWLEDGMENTS

I would like to express my gratitude to my advisor, Professor W. G. Knauss, for his support, suggestions and encouragement during this investigation. I would also extend my appreciation to Professor Ravichandran and Professor Rosakis for their valuable assistance in my research.

I wish to thank my colleagues Dr. Hongbing Lu, Dr. Tony Deng, Limdara Chea, Sandeep Sane and post doctoral scholars Dr. Alfons Noe and Dr. Allan Zhong for their useful input in this project. I would also like to thank my officemates Demir Coker, Javier Gonzalez, Pradeep Guduru, Sangwook Lee, Omprakash Samudrala and other graduate students for their friendship, valuable advice and for making my stay at Caltech a memorable experience.

This project was initiated under ARO grant DAAL03-92-G-0192 and previous participants were supported under AASERT grant DAAH04-93-G-0387. I would like to thank for this support of the research.

ABSTRACT

An experimental method for visualizing and analyzing the propagation of plate stress waves in a brittle plate is developed. A procedure has been developed to cast Break-Away glass (a low molecular weight polystyrene material) plate specimens in an open mold. The specimens are loaded with short duration (200 μs) stress pulses on one edge by an electromagnetic stress wave generator. The propagating stress waves generate out-of-plane deformations on the specimen surface, which are observed using Twyman-Green interferometry. The fringe patterns created by the propagating stress waves are captured using a high speed camera – pulsing laser combination at 4 μs intervals.

A generalized "Fringe Analysis Procedure" is developed to subtract the reference interferogram from the subsequent interferograms. The "Fringe Analysis Procedure" employs a fringe edge detection algorithm to obtain the sharp edge lines of the fringes in an interferogram. A digitizer is used to extract points on these edge lines and assign them fringe numbers. The "griddata" option in the commercial software "Matlab" is utilized to interpolate the deformation field on to the nodes of a uniform grid. The field values at these nodes in the reference image are then subtracted from corresponding values in the subsequent images to obtain the actual deformation patterns generated by the propagating stress waves. The "Fringe Analysis Procedure" has eliminated the subjective element introduced by human judgment in manual fringe tracing procedures.

The developed experimental method and the image analysis technique is used to investigate the propagation of stress waves in Break-Away glass plate specimens.

TABLE OF CONTENTS

LIST OF FIGURES

LIST OF TABLES

1. Introduction

The armor of a tank protects it from incoming high velocity projectiles such as gunfire and missiles. At present, the armor surrounding the tanks is made of high strength steel that can absorb large impact energy. In the recent past, ceramic materials having characteristically high compressive strength are being considered for use in several such engineering applications. There is a growing interest in the US Army to utilize these ceramic materials as the armor for the next generation of tanks to realize better protection. However, ceramics are brittle in nature and exhibit poor performance in tensile loading due to relatively low fracture toughness. Also, like any other material, with aging or enduring gunfire in the past, the material can develop micro-cracks, which then grow in time, coalesce, and lead to discontinuities in the material. High energy impact by shells or rockets results in local fragmentation of the material which creates an essentially discontinuous but intact armor medium. When a projectile hits such a cracked region in the armor, it produces stress waves that propagate through the discontinuous medium. The fragmented material should be able to transmit the high impact energy to the neighboring regions through these discontinuities, possibly by stress waves, to effectively absorb the impact. A number of numerical models of the stress wave propagation in the fragmented zone have not yielded satisfactory results. It is, therefore, essential to understand the interaction of these stress waves in brittle, cracked medium, using experiments, to accurately model the material and to predict the protection the brittle ceramic armor would provide to the tanks. The aim of this project is to observe and model the interaction of stress waves with material discontinuities as they propagate through a cracked, brittle medium, schematically shown in figure 1.1a*.

To simulate this interaction of stress waves in a cracked zone in the laboratory and to readily control the introduction of cracks into a specimen, it is desirable to choose a material of low fracture strength. For this reason a low strength, highly brittle polymer

---

* All figures are placed at the end of respective chapters.

glass, known in the literature as Break-Away glass, and commercially known as "Candy glass" was selected. The material can be easily stressed to its maximum failure strength of 5 MPa using an electromagnetic stress wave generator available at GALCIT. As a first step in this project to develop suitable analysis procedures, a simplified case is considered as shown in figure 1.1b. Stress waves are imparted at the top edge of the Break-Away glass specimens without any material discontinuities using a Lorentz stress wave generator, and the out-of-plane deformation filed generated by the propagating waves are analyzed.

The Lorentz stress wave generator consists of a capacitor bank that produces a surge of current over a short duration of time through a double-folded copper strip. The induced magnetic fields in each leg interact with the current flowing through the other leg to produce a pressure field that forces the conductors apart. A loading device was designed and fabricated for imparting a controlled planar stress wave, induced by the current in the conductors, to the top edge of the specimens.

Photoelasticity and Twyman-Green interferometry are two potentially suitable optical techniques for analyzing the propagation of waves. While photoelasticity produces no initial fringe pattern, the material needs to have a high characteristic material fringe value to be able to retrieve meaningful data from experiments. Furthermore, photoelasticity averages the stress field over the thickness and is sensitive to variation in the thickness of the specimen over the field of view. Twyman-Green interferometry, on the other hand, records the out-of-plane deformation field on the surface of the specimen. The fringe density obtained depends on the magnitude of the deformation field and the wavelength of light used. After the initial tests, which are described in detail in chapter 2, Twyman-Green interferometry was chosen to record the fringe patterns created by the out-of-plane deformations in the specimens. An inherent drawback of Twyman-Green interferometry technique is that it may give a fringe pattern even when there is no stress in the specimen, due to the initial surface irregularities on the specimen. This reference image needs to be subtracted from the subsequent images to obtain the actual out-of-plane deformations generated by the

stress field. Various attempts were made at subtracting the reference image from the subsequent images. Chapter 3 summarizes the merits and drawbacks of the various software and procedures that can be employed to carry out the image analysis.

While the strength characteristics of Break-Away glass are particularly desirable to be able to introduce cracks in a plate specimen, it also turned out that very little was known about its physical and mechanical behavior. This lack of knowledge made it difficult to find a repeatable method for manufacturing specimens of desired shape and size as a prerequisite for setting up experiments to observe the wave propagation in this material. However, a series of studies[1,2,3] characterized the physical, chemical and mechanical properties of candy glass. The results obtained in these investigations are summarized in table 1.

The earliest attempts in this project were directed at producing plate specimens with optical surface quality. Several attempts to machine the material by milling, grinding, sanding as well as cutting with a hot knife did not produce satisfactory results. The main impediment was the extraordinarily low strength and brittle nature of the material. Due to these difficulties in machining, efforts were made to cast the Break-Away glass in a mold, as was being accomplished in previous studies with PMMA plates[4]. However, these attempts did not yield satisfactory results, because the cast specimen broke into several pieces during cooling to less than 20 ^{o}C below the glass transition temperature, even with the use of mold release agents. It was observed that the specimens were breaking at around, 40 - 50 ^{o}C, just below the glass transition temperature (64 ^{o}C) as a result of the residual stress generated in the cool-down process and glass adherence during solidification. Teflon tapes were applied on the edges of the base mold and on the sides to prevent stress build-up. Finally, a repeatable procedure was developed that produced flawless specimens in a mold as presented in detail in chapter 2 and Appendix of this thesis.

The specimens are loaded with a short duration stress pulse by the capacitor bank and the loading device. The fringe patterns produced by Twyman-Green interferometry technique are captured at regular intervals using a high-speed camera. The actual surface deformations are obtained by subtracting the reference fringe pattern from the subsequent images. The analyzed images provide insight into the effects of a stress pulse propagating through a continuous brittle medium.

Table 1 : Characteristic Properties of Break-Away Glass Material [1,2,3].

	MEAN.	STD. DEV.	RSS ERROR.
Density (ρ) (Kg / m^3)	1050	50 (4.8%)	
Shear Wave Speed (C_s) (m / s)	1174	11 (0.9%)	
Normal Wave Speed (C_n) (m / s)	2382	18 (0.8%)	
Poison's Ratio (ν)	0.34		0.01 (1.5%)
Elastic Modulus (E) (GPa)	3.88		0.19 (5.0%)
Shear Modulus (G) (GPa)	1.45		0.07 (5.1%)
Bulk Modulus (K) (GPa)	4.03		0.22 (5.4%)
Maximum Tensile Strength (σ_{max}) (MPa)	5.0		1.0 (20%)
Glass Transition Temperature (T_g) (^{o}C)	64		
Boiling Point (T_b) (^{o}C)	325		
Melting Point (T_m)	Material softens at approximately 120 ^{o}C and becomes a very viscous liquid at about 130 ~ 140 ^{o}C.		
Material Composition	Polystyrene mixture with 3000 and 100,000 MW components.		

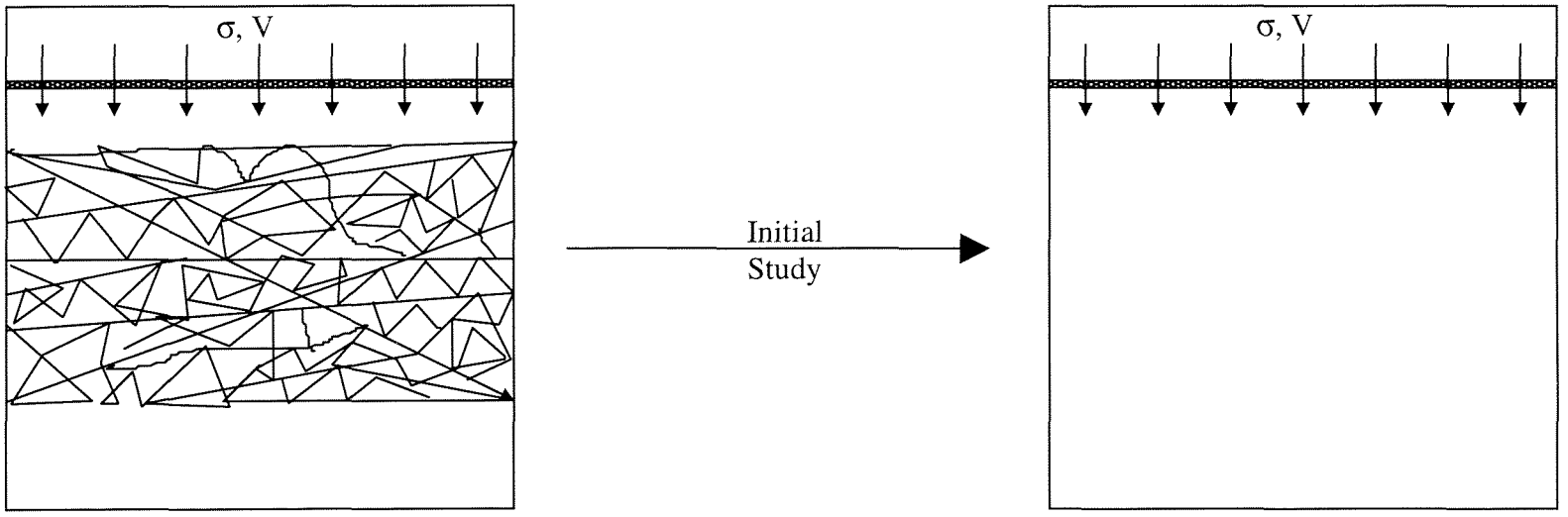

Figure 1.1a : Wave interaction in a fractured medium.

Figure 1.1b : Wave propagation in a continuous medium.

2. Experimental Procedure

A schematic diagram of the experimental setup used in this study is shown in figure 2.1. It consists of a pulsing laser and an optical setup to capture fringe patterns created by propagating waves in the specimen. The specimen is cast in an open steel mold and the flat side of the specimen is coated with Aluminum to provide a reflective surface. The specimen is loaded on one edge by the Lorentz force generator. The triggering of the capacitor bank, the laser and the high-speed camera are synchronized by a circuit of delay generators, amplifiers and function generators. Each aspect of the experimental setup is described in more detail in the following sections.

2.1 Specimen

In the Introduction, it was mentioned that thermal stress build-up, together with the relatively low strength of the Break-Away glass, led to the premature fracture of specimens. Also during the cooling process, when the material crosses the glass transition temperature, it sticks to the mold material, especially to the edges of the mold, thus inducing thermal residual stress. This problem is avoided by applying a thin coat of Teflon spray on the mold and attaching Teflon tapes along the sides of the mold. In addition, the sides are loosened at around 75 °C, when the material is still soft but viscous enough not to flow out of the mold. The cooling rate was also adjusted by experimenting with a wide range of rates. The specimen is cooled at a moderate rate (around 7 °C / hour) down to 65 ~ 70 °C, after which it is cooled very slowly (less than 3 °C / hour) below 65 °C through the glass transition. Though this operation enlarged the number of unbroken specimens, it was far from being a reliable method. In some trials the cast plate was removed from the mold at temperatures of 45 ~ 50 °C. However, the material was still soft at this temperature and stuck to the mold. After several attempts at varying the cooling rate, soaking and placing Teflon tapes in various locations, a repeatable procedure was developed to produce plate specimens of 300 × 300 mm

dimension and about 6 mm in thickness as described in the Appendix. The specimens possess an optically smooth though not optically flat surface over its central region of 75×150 mm dimension.

2.2 Stress Wave Generator

Stress waves are generated at one edge of the plate specimen through a Lorentz stress wave generator, which consists of a capacitor bank, a copper strip and a loading device designed at GALCIT.

2.2.1 Principle of the Loading Method

The electro-magnetic loading device (capacitor bank) is initially charged to a preset voltage. The capacitor bank, when triggered, discharges a current pulse through a doubled-up conductor (copper strip) which is inserted in between one edge of the specimen and a rigid back-up support. When the current flows through the loop, each leg of the strip generates a magnetic field surrounding it, the field being normal to the direction of flow of current in each leg of the strip as shown in figure 2.2. The current in each leg interacts with the magnetic field generated in the other leg to produce an electro-magnetic pressure that forces the conductors apart. An expression for the electromagnetic pressure generated for the case of two sheets of same width, each carrying the same current in the opposite direction is obtained as follows.

In an infinite width geometry (w>>d in figure 2.2) the magnetic field $\vec{B}$ is uniform across the width of the strips. In this region $\vec{B}$ is expressed as

$$\vec{B} = B_z \vec{e}_z ,$$

where

B_z : Magnitude of the magnitude field

$\vec{e}_z$: Unit vector in the z-direction.

Ampere's law states that

$$\oint \vec{B} \cdot d\vec{s} = \mu_o I, \tag{2.1}$$

where

$\vec{B}$: Magnetic flux density

I : Total current flowing through each strip

μ_o : Permeability of free space ($4\pi * 10^{-7}$ Wb / Amp^2)

If a loop is taken around the cross section of the copper strip shown as dotted line in figure 2.3, under the assumption that the separation between the strips, d, is much smaller than the width of the strips, w, equation 2.1 simplifies to

$$B_z \, 2w = \mu_o I$$

or
$$B_z = \mu_o I / 2w \tag{2.2}$$

where

w : Width of the copper strips

d : Separation between the strips.

Adopting Lorentz's law

$$\vec{f} = \vec{i} \times \vec{B}$$
$$= i B_z \vec{e}_y \tag{2.3}$$

where

$\vec{f}$: Force per unit volume exerted on strip 2 by strip 1

i : Current density =I / (w . t)

t : Thickness of each strip.

Upon substituting the expression for B_z from equation 2.2, the magnitude of the force intensity induced between the strips becomes

$$f = \mu_o \frac{I}{w \cdot t} \frac{I}{2w} . \tag{2.4}$$

The pressure generated by this current is obtained by integrating the force density over the thickness of the strips

$$P = \int f \cdot d(thickness)$$

which results in

$$P = \frac{\mu_0}{2} \left(\frac{I}{w} \right)^2 . \tag{2.5}$$

This is the pressure created by the current in sheet 1 on sheet 2 which results in a compressive stress pulse on the specimen. For the case where the width to separation ratio (w/d) is not negligible, the expression can be written as[5]

$$P = \frac{\mu_0}{2\pi} \left(\frac{I}{w} \right)^2 * \left[2 \tan^{-1} \left(\frac{w}{d} \right) - \left(\frac{d}{w} \right) \ln \left(1 + \frac{w^2}{d^2} \right) \right] \tag{2.6}$$

For the limiting case w/d $\rightarrow \infty$, the expression yields the same result as in equation 2.5. In this investigation, the separation between the strips is very small compared to their width and hence equation 2.5 is used to evaluate the magnitude of the stress pulse generated in the specimen.

2.2.2 Capacitor Bank

The stress pulse propagating through the specimen takes the shape of the electro-magnetic pressure generated by the copper strip, which in turn is controlled by the current flow in the strip, as shown in equation 2.5. In order to control the time history

of the current, several capacitors are arranged with inductor coils as shown in figure 2.4. The circuit consists of 12 loops of sub-circuits with capacitors and inductors. The first loop has a capacitor of 14.5 μF capacitance and an inductor coil. The next ten loops each have two capacitors and an inductor. The last loop connects the copper strip to three capacitors of 14.5 μF capacitance through an ignitron switch. When the ignitron switch is triggered, the three capacitors in the last sub-circuit yield a large current with a short rise time in the copper strip. The inductor coils in the subsequent sub-circuits delay the discharge of capacitors in those loops. As the delayed discharges add to the current in the copper strip, the initial current is sustained over a long period of time (200 μs). The magnitude of pressure generated by this pulse can be calculated using equation 2.5. The inductor coils are specially designed to yield a reasonably uniform stress pulse with a very short rise time. The shape of the stress pulse is sensitive to various inductance and capacitance values in the circuit and can deteriorate in time due to oxidation and aging of various components of the circuit. The time history that is derived from the circuit for a voltage setting of 1800 Volts is plotted in figure 2.5. The initial rise time obtained is less than 20 μs and the pulse duration is about 200 μs. The stress pulse has an initial peak of 0.86 MPa and levels at around 0.42 MPa and stays at this value for most of the pulse duration.

A Rogovski coil is attached at the exit of the capacitor bank to measure the current flow. It is essentially an inductor coil which senses the rate of change of current in the copper strip. The output of the Rogovski coil is passed through an integrator circuit to obtain the actual shape of the current pulse passing through the copper conductor. The voltage reading from the Rogovski coil needs to be calibrated in terms of the current in the copper strip.

Rogovski Coil Calibration

In order to calibrate the output of the Rogovski coil, the conductor is connected to only one of the capacitors and one inductor in the capacitor bank. The resulting output from

this *L-C* circuit is shown in figure 2.6. The noise found in the beginning of this plot is due to the electromagnetic disturbances created by the ignitron when it is switched on. The output signal is a decaying sine wave with a constant time period. The ratio of magnitudes of successive peaks also remains a constant. The amplitude of the current at quarter time period for an *L-C* circuit can be expressed as[6]

$$I_{T/4} = V\,C\left(\frac{2\pi}{T}\right)\left(\frac{A_3}{A_1}\right)^{\frac{1}{4}} \qquad (2.7)$$

where

$I_{T/4}$: Current at quarter time period, in amperes.

V : Capacitor charge, in volts.

C : Capacitance, in Farads (= 14.5 μF).

T : Time period, in seconds.

$\frac{A_3}{A_1}$: Ratios of successive peaks of the same sign in the signal.

From tests for a voltage setting of 1800 Volts, $\frac{A_3}{A_1}$ and T were found to be

$$\frac{A_3}{A_1} = 0.7042$$

$$T = 50.75\ \mu s$$

which yields, from equation 2.7,

$$I_{T/4} = 2960 \text{ amperes.}$$

This value of $I_{T/4}$ causes a known voltage of 26.288 milivolts from the Rogovski coil. Hence 1 volt of Rogovski coil output is related to the actual current in the conductor in amperes as

$$\textbf{1 volt of Rogovski Coil output} = \textbf{1.126} \times \textbf{10}^{\textbf{5}}\ \textbf{amperes current in copper strip} \qquad (2.8)$$

The magnitude of the current in the copper strip depends mainly on the voltage setting in the capacitor bank, and the arrangement of inductors and capacitors determines the time function shape of the current. Tests show that variation in the length, width and thickness of the copper strip has little effect on the current history. The magnitude of the stress pulse can thus be controlled by the voltage controller through which the capacitor bank is charged. The following relations show the qualitative dependence of magnitude of the stress pulse on the voltage setting in the controller.

$$I \propto V$$
$$\sigma \propto V^2 \tag{2.9}$$

where,

I : Current in the copper strip

σ : magnitude of the stress pulse generated

V : Voltage setting in the capacitor bank.

2.2.3 Loading Device

The Lorentz stress wave generator has been extensively used at GALCIT in earlier investigations to generate uniform stress pulses. However, in most of the previous applications [4,6,7], the copper strip was inserted into a crack at the center of a specimen. When a current is passed through the copper strip the two legs of the loop are forced apart to open the crack. In the present application a compressive stress pulse needs to be generated at one edge of the plate which propagates through the specimen. To achieve this goal, the loading device has been modified as shown in figure 2.7. It consists of two holding blocks made of PMMA, with slots cut into them to hold the specimen in position. The folded copper conductor is placed inside the upper slot. It is held by two supports pressing on both ends to make sure the two legs of the strip are close to each other. The specimen is placed between the two blocks with enough clearance to avoid any initial stress in the specimen. The upper edge of the specimen is

bonded to the surface of the copper strip to ensure that a spatially uniform stress pulse is generated across the width of the specimen.

Copper Strips

When the copper strips are cut (by shearing) from a big sheet, they curl due to the plastically generated residual stresses. The strips are annealed before using them in the loading device. For this purpose, a slot or recess has been cut into a rectangular steel block; the strip is placed into the recess and pressed with another steel block while being heated in an oven at 200 ^{o}C for three hours. When cool, the strip is stretched under a dead weight, thus further straightening it. An insulation tape is wrapped around the strip along its length. A normal ½ inch wide Scotch tape is used for this purpose. The strip then is folded and placed in the holding slot in the back-up block of the loading device.

2.3 Experimental Technique

Photoelasticity and Twyman-Green interferometry are two widely applied full field optical techniques that have been frequently used at GALCIT to observe dynamic deformation of materials. Hence, these two techniques were possible choices for observing the stress wave propagation in this project.

In order to be able to use photoelasticity, the material must have good photoelastic sensitivity, that is a high characteristic material fringe value f_{σ}. A 6.4 mm thick plate specimen was tested to calibrate the characteristic material fringe value (f_{σ}) of the Break-Away glass material. The plate was statically loaded with a point load at one edge and the fringes observed using photoelasticity were captured. Figure 2.8a through figure 2.8i show the fringe patterns created near the tip of the load at load increments of 43.2N. A He-Ne laser light of 633 nm wavelength was employed to provide a light

source for photoelasticity. Around 2 to 3 fringes were recorded before the specimen broke. Comparing this result with the analytical solution of a point load on a half space, the material fringe value (f_σ) for break away glass, for a light of wavelength 633nm is estimated to be

$$f_\sigma = 1.8 \times 10^4 \text{ N/m/fringe} \qquad \text{for } \lambda = 633 \text{ nm.}$$

The pulsed laser source, to be employed in dynamic experiments, produces a laser light of wavelength 514 nm. The material fringe value of breakaway glass for this wavelength can be calculated to be

$$f_\sigma = 1.45 \times 10^4 \text{ N/m/fringe} \qquad \text{for } \lambda = 514 \text{ nm.}$$

The failure strength of Break-Away glass is 5 MPa. That means when a specimen of 6 mm thickness is loaded with a stress pulse of magnitude of the order of the maximum strength of the material, only 2 to 3 fringes would be recorded, which would not yield adequate information required in this study.

For this reason Twyman-Green interferometry was pursued to observe the propagation of waves. The associated arrangement of the laser and the optics used in this setup are shown in figure 2.1 The laser light is expanded through a collimator to a 50 mm diameter beam. The expanded beam passes through a beam splitter placed at 45° inclination angle to the path of the beam, which divides the light into two beams. Light passing straight through the beam splitter falls on the specimen and is reflected back. The other part of the light traversing at right angle to the path of the light is reflected back by a plane reference mirror. The reference mirror is placed at the same distance from the beam splitter as the specimen. The reflected beams from the specimen and the reference mirror interfere to produce a fringe pattern which is captured on the image plane of the high speed camera through a lens and shutter arrangement in the camera.

The phase of the reflected light from the specimen contains information about the specimen surface deformation. If two points on the specimen surface are not at the same optical distance from the beam splitter, the rays reflected from these two points possess different phase. These rays interfere with the light reflected from the reference mirror to create constructive or destructive interference producing white and black fringes respectively.

2.4 Synchronization of Events (Electronics)

The dynamic experiment lasts for only a few hundred microseconds. Hence, the synchronization of the opening of the shutter, the triggering of the capacitor bank and the pulsing of laser play a crucial role in the success of the experiment. As a consequence, the delays in triggering of various instruments needed to be calibrated.

Camera

Before triggering, the air turbine of the high speed camera is brought to steady rotation. At a manifold pressure setting of 15 psi in the camera pressure gauge, 128 exposures of full 35 mm film size, exposed at 7 μs intervals are obtained. However, the area exposed per frame on the film track can be reduced to a smaller but reasonable size (typically 15 mm and some gap between exposures) to allow an increase in the framing rate. An image size of 15 mm (for the actual size of 50 mm on the specimen surface) on 100 TMAX KODAK film provides good resolution. In this study the field of view is a 25×30 mm rectangular area in the central region of the specimen. The framing rate is set at 250,000 frames per second. An exposure time of 8 ns per frame via the pulsed laser gives less than 0.2% shift (blur) on the film track. The film is exposed for 600 μs giving around 150 pictures. These parameters are set in the pulse generator (H-P model) and the brag cell controller of the laser; the turbine rotates at a sufficient speed to avoid picture overlapping.

Shutter

In order to avoid light leakage, a copal shutter is used to open and close access to the optical track. From the above mentioned parameters, one needs to have the shutter open for at least 600 μs. Due to the relative difficulty in controlling mechanical shutters to such precision, the shutter is left open for 2000 μs. It has been concluded from experience that any light leakage during this comparatively large time does not affect the image quality significantly. In addition, there is a 5000 μs delay in the opening of the shutter after triggering. This is very important to note, as the other events also need to be delayed by the same time or more.

Laser Pulsing

The triggering of light from the laser follows the external trigger signal input into it virtually simultaneously. A pulse generator is triggered around 5000 μs after the copal shutter is triggered. The pulse generator (Rutherford model) produces a single square pulse of 600 μs duration, which is used as a gate input to another pulse generator (Hewlett-Packard or H-P model). The HP pulse generator transmits pulses at 4 μs intervals to the laser unit when the gate input is on. The brag cell controller sets the width of each pulse. For this investigation, the width of each pulse is set at 8 ns, which is the minimum possible setting in the controller. Thus around 150 laser pulses of 8 ns duration each, at an interval of 4 μs, are obtained when the copal shutter is open.

Capacitor Bank

Similar to the laser, the capacitor bank is also triggered around 5000 μs after the copal shutter is opened. The capacitor bank has a mercury switch (ignitron) that needs a 2.0KV signal for on-switching. Various intermediate voltage step-ups are used for this purpose as shown in figure 2.1. The ignitron is triggered by a Thyratron (250V -

2.2KV), which itself is triggered by a relay generator (10 - 250 V), which in turn is triggered by a 10 Volts signal from a delay generator.

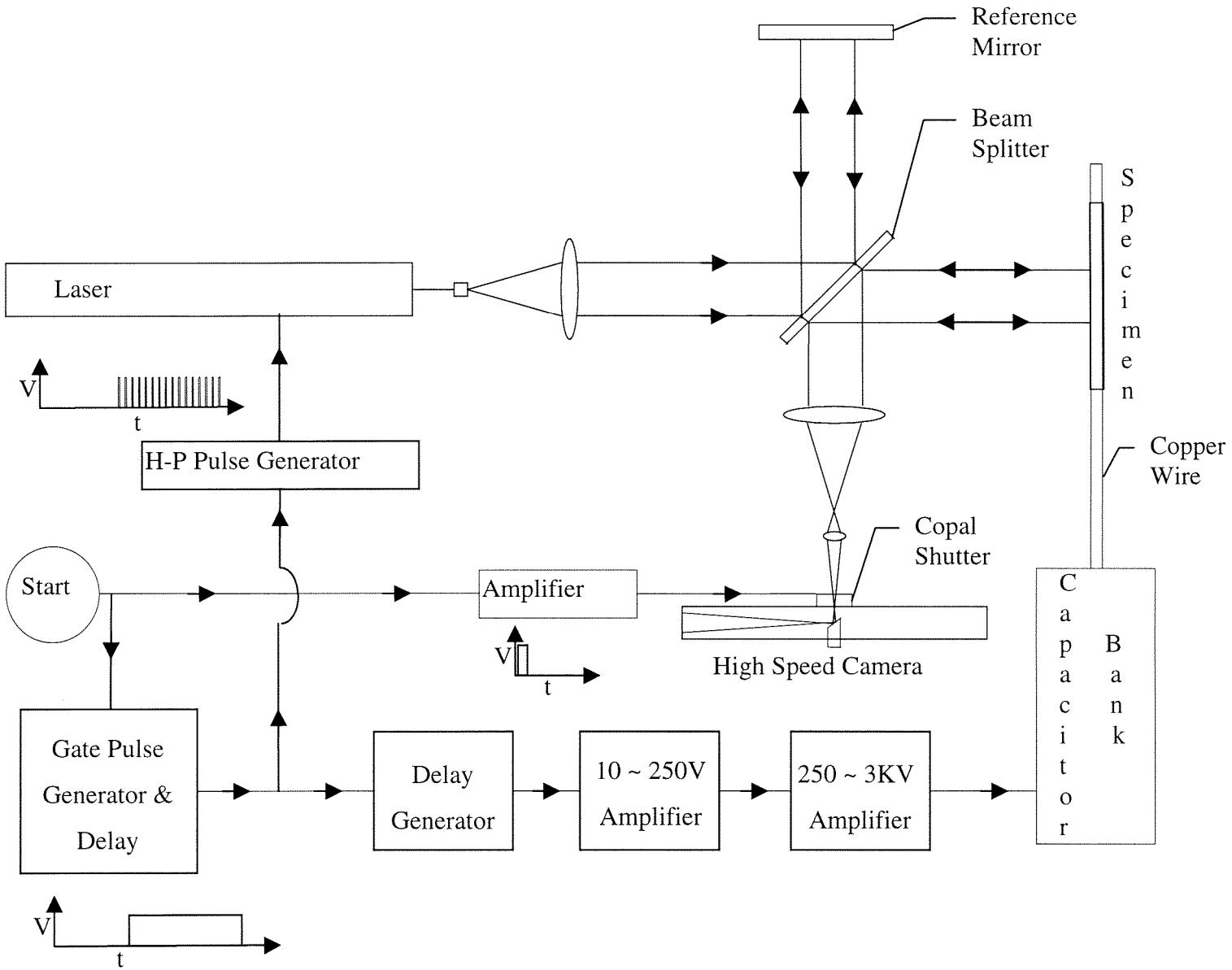

Figure 2.1 : Schematic diagram of the experimental setup.

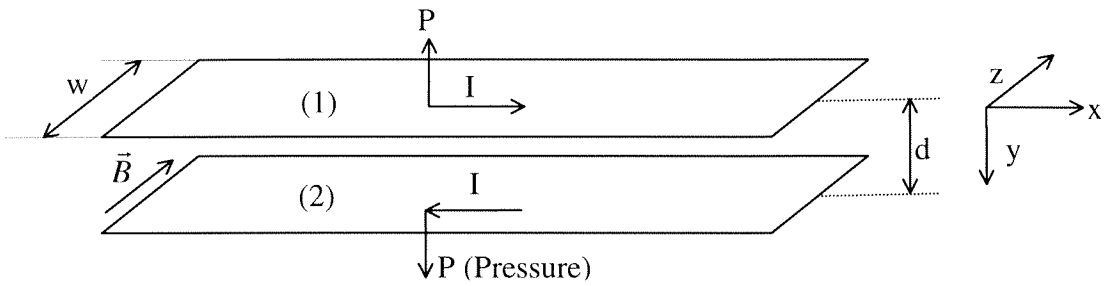

Figure 2.2 : Interaction of magnetic field and current in the copper strips.

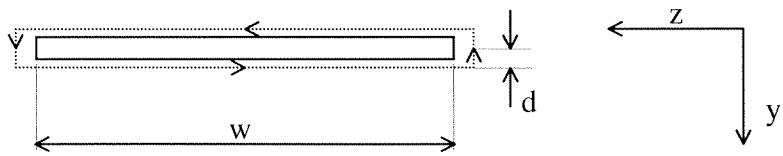

Figure 2.3 : Cross section of the conductor.

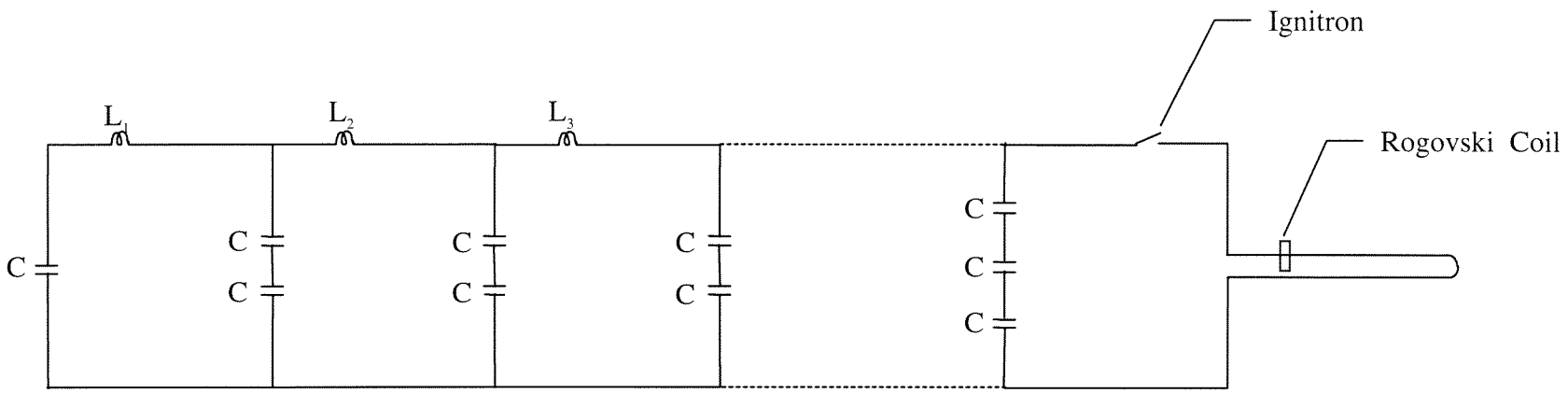

Figure 2.4 : Sketch of capacitors and inductors arrangement in the capacitor bank.

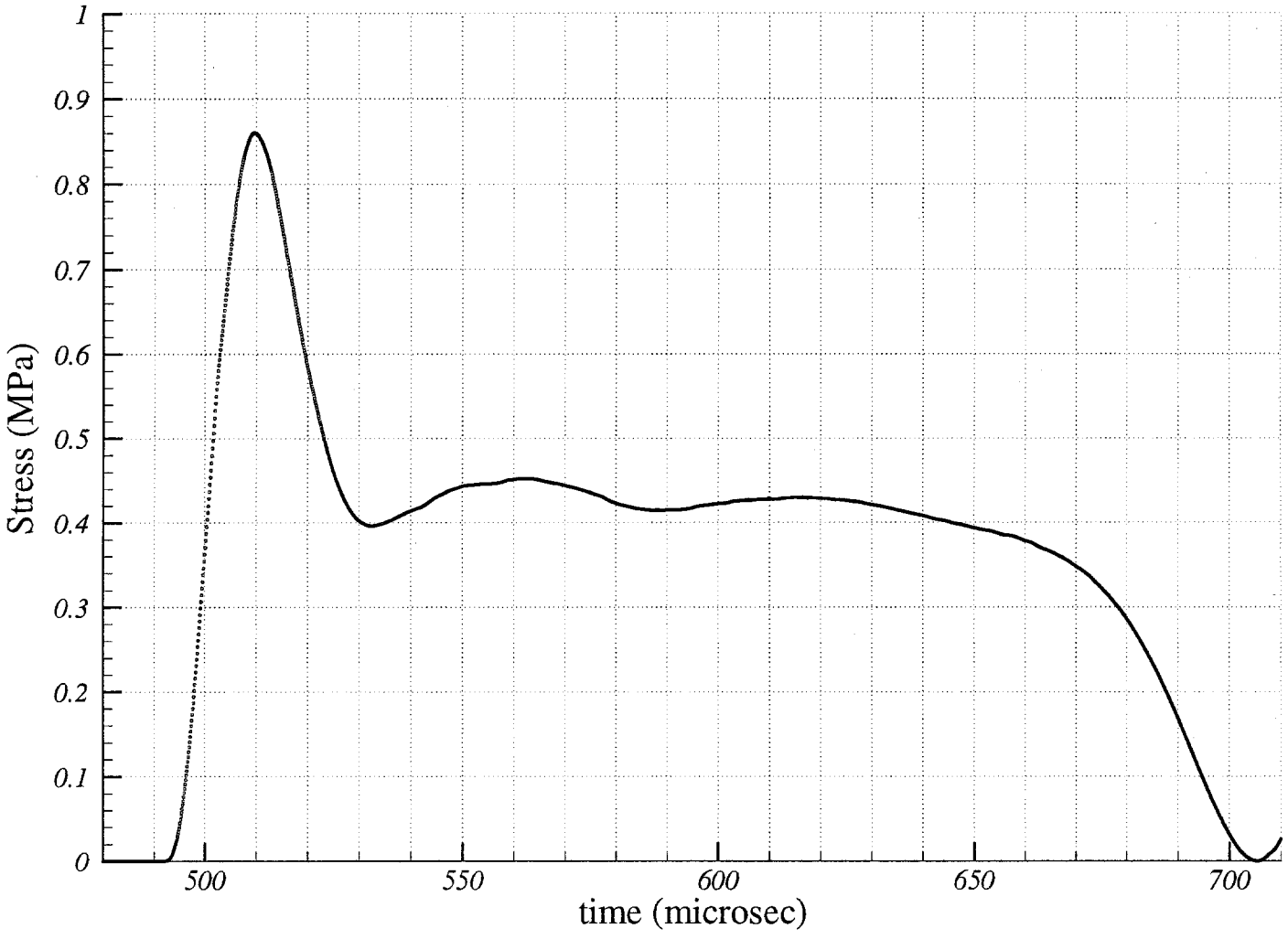

Figure 2.5 : Time history of the stress pulse imparted on the specimen.

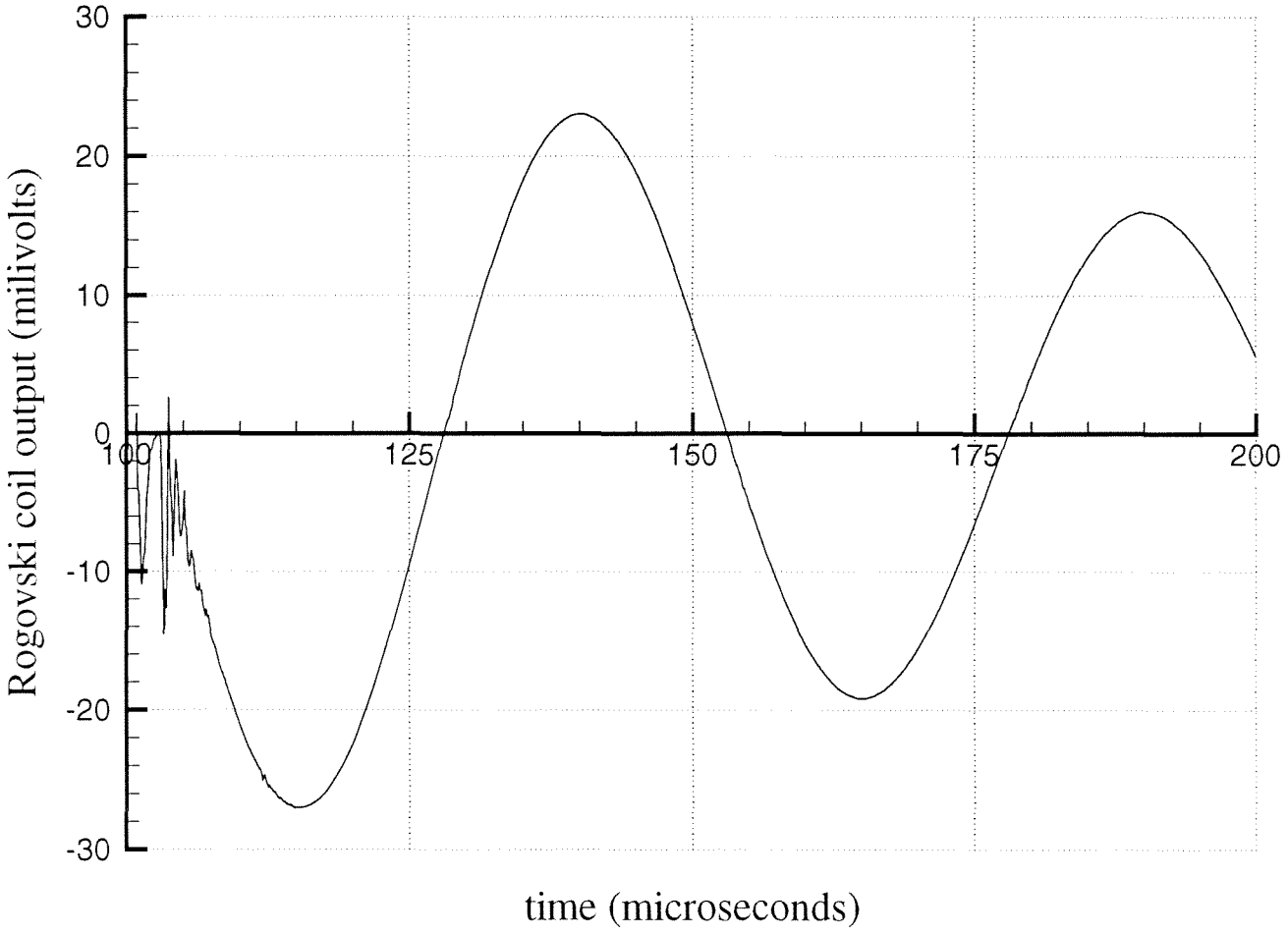

Figure 2.6 : Output from Rogovski coil for a single capacitor-inductor configuration.

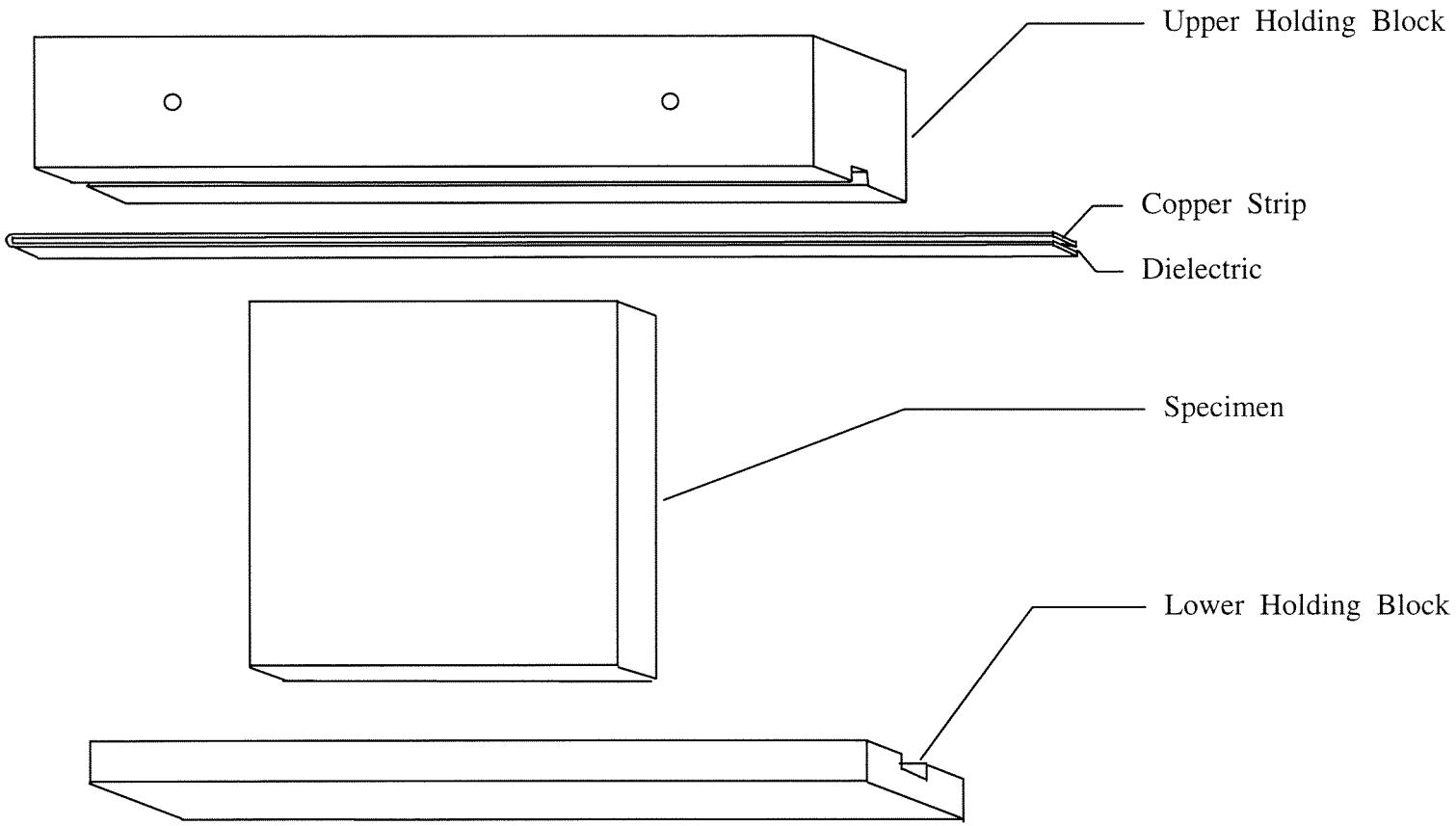

Figure 2.7 : Loading device.

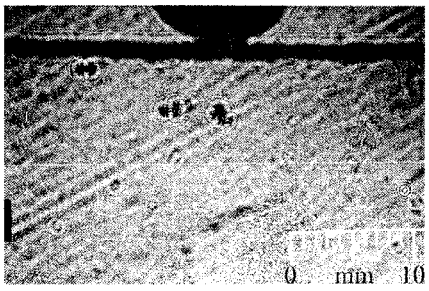

Figure 2.8a : Photoelasticity image at no load.

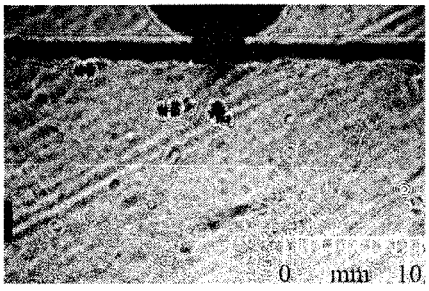

Figure 2.8b : Photoelasticity image at 43.2 N load.

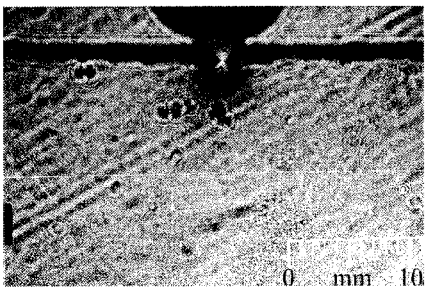

Figure 2.8c : Photoelasticity image at 86.4 N load.

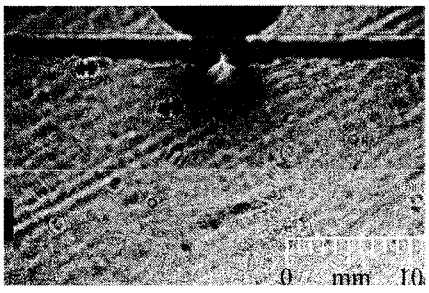

Figure 2.8d : Photoelasticity image at 129.6 N load.

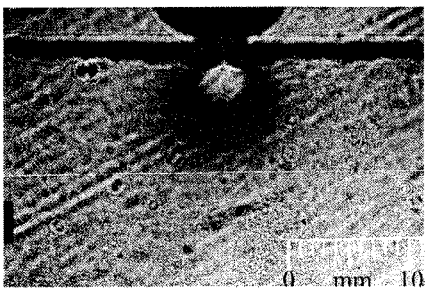

Figure 2.8e : Photoelasticity image at 172.8 N load.

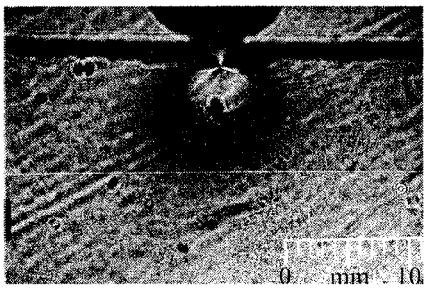

Figure 2.8f : Photoelasticity image at 216 N load.

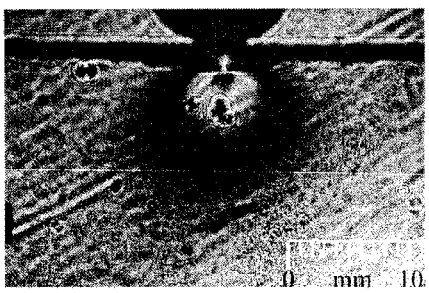

Figure 2.8g : Photoelasticity image at 259.2 N load.

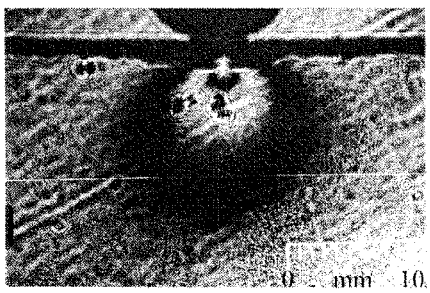

Figure 2.8h : Photoelasticity image at 302.4 N load.

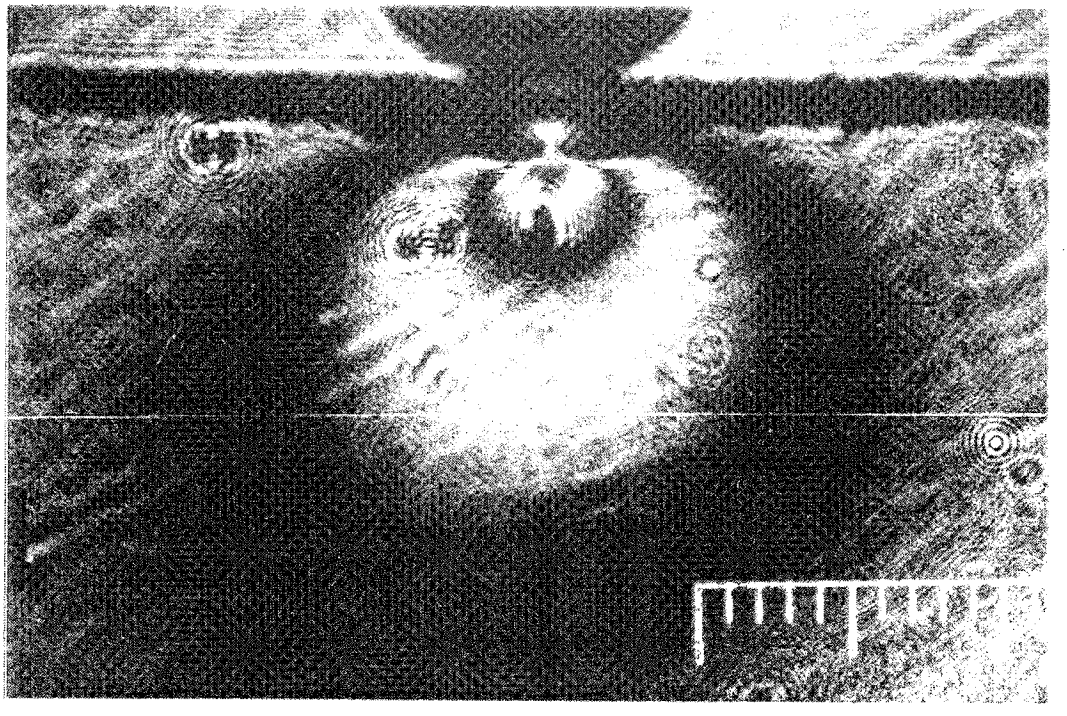

Figure 2.8i : Photoelasticity image at 305 N load when the material breaks.

3. Image Analysis

The fringe patterns created by propagating waves in the specimen are captured on TMAX-100 Kodak film using the high speed camera. A qualitative comparison of successive images clearly shows disturbances propagating through the field of view. To obtain quantitative results like the speed and magnitude of these propagating surface deformations, the images are further analyzed.

In all the tests conducted to date, fringe patterns are observed even before any stress wave has reached the field of view. These patterns are referred to as the reference fringe pattern and are created by initial irregularities of the specimen surface. In spite of several attempts to obtain an optically flat specimen surface, thermal stress, built up in the specimen during the cooling process, leaves unavoidable irregularities on the surface, which result in this initial fringe pattern. This reference image needs to be subtracted from the subsequent images in order to get meaningful data from the images.

To generalize the subject matter, most of the full field optical techniques used in dynamic experiments produce interferograms, which need to be processed to extract meaningful data. In general, fringe patterns in the interferograms represent the field information such as the out-of-plane deformation field in Twyman-Green interferometry, the maximum shear stress field for isochromatic fringes of photoelasticity and the gradient of triaxial stress field in the coherent gradient sensing technique. Though the availability of powerful pulsing lasers and advanced high speed cameras has considerably improved the time required in conducting an experiment, most often the interferograms are analyzed manually. A typical dynamic experiment produces several images with many fringes in each image, which makes the image analysis a time-consuming process. Though the edge between white and black fringes should be ideally a distinct line, in reality these two regions slowly merge onto each other, making it difficult to isolate the regions and identify their edges or centers. This inaccuracy can lead to erroneous data. Analysis of data from interferometric fringe

patterns requires automation in order to avoid both the tedium of manual data extraction as well as to reduce the inaccuracy introduced by human error. The goal is to be able to input the scanned images into a computer, which runs an algorithm to trace the edges or centers of the fringes accurately and provides the field value at any point on the domain using an interpolating function, thus requiring minimal interaction with the user.

A number of automatic fringe analysis programs have been discussed in the literature. Typically, these techniques employ fringe-tracing algorithms to trace the centers of the fringes. The simplest approach is to scan the images using horizontal and vertical scan lines, which determines the mid-points of dark and bright regions[8]. However, this algorithm fails when the fringes run parallel to the scan lines. The other techniques use fringe peak detection algorithms and have been successfully applied to locate the center of fringes in some applications[9]. Nevertheless, these techniques cannot be extended to any general interferogram analysis. The fringe patterns obtained in different applications vary widely in terms of fringe density, uniformity of intensity distribution, noise level et cetera and a general-purpose computer image processing algorithm is yet to be developed.

In this study a new image analysis procedure is developed in an effort to automate the analysis of interferograms. It eliminates the inaccuracy introduced by human judgment in locating the centers of the fringes. The procedure has been successfully applied to analyze interferograms obtained in the present investigation. It can be extended to any full-field optical technique that produces fringe patterns due to interference of light.

3.1 Interference of Light

The schematic configuration for Twyman-Green interferometer is shown in figure 3.1. A detailed description of the technique can be found in *Principle of Optics,* by Born and

Wolk[10] and in *Optics,* by Hecht[11]. The intensity distribution for the interference of two lights of same amplitude is expressed as[12]

$$I = 4A^2 \sin^2 \left(\frac{\delta}{2} \right) \tag{3.1}$$

where

I : Intensity at any point (x,y)

A : Magnitude of the original light

δ : Difference of phase between the reference light and the reflected light from point (x,y) on the specimen.

The expression in equation 3.1 shows that the interferogram contains both the magnitude and phase information of the light reflected from the specimen surface. The phase difference between the two interfering light creates the pattern of black and white fringes. If the phase difference is such that $\delta = 0, 2\pi, 4\pi, \ldots$, then it results in a constructive interference generating a maximum intensity of amplitude $4A^2$ at that point. If, on the other hand, $\delta = \pi, 3\pi, 5\pi, \ldots$, it leads to a destructive interference and the intensity at that point is 0. The intensity distribution between these two regions follows a sine-squared function.

In the Twyman-Green interferometer, the out-of-plane surface deformation (w) on the specimen surface effects the path traversed by the reflected light by twice its magnitude (2w). A change in the light path equal to the wavelength of the light (λ) is equivalent to a 2π change in the phase of the light. Mathematically one has

$$\delta = 4\pi \cdot \frac{w}{\lambda} \tag{3.2}$$

where

δ : Phase difference between the two lights

w : Out-of-plane deformation at any point (x,y)

λ : Wavelength of light used in the experiment.

Equation 3.1 can thus be rewritten as

$$I = 4A^2 \sin^2 \left(\frac{2\pi w}{\lambda} \right) \tag{3.3}$$

The interference of light produces a light fringe for w = 0, $\frac{\lambda}{2}$, λ, $\frac{3\lambda}{2}$, . . .; and a dark fringe for w = $\frac{\lambda}{4}$, $\frac{3\lambda}{4}$, $\frac{5\lambda}{4}$, . .. In other words, each fringe order on the interferogram represents a $\frac{\lambda}{2}$ out-of-plane deformation on the specimen surface.

3.2 Fringe Analysis Software

The first attempt to subtract the reference image from subsequent images was performed by using a software developed at GALCIT, namely "Fringe Analysis Software"[13], that extracts the magnitude and phase information from the interferograms and rebuilds the fringe field. The software was successfully used to subtract images in the study of crack propagation in PMMA[4]. In this method, the images obtained from experiments are scanned using an *H-P* model desk scanner. A 75 dots per inch resolution provides good picture quality for the 8 × 10 inches prints. A window is chosen in each image, which represent the same region on the specimen. The images in the windows are cropped and these images are used for further analyses.

The Fringe Analysis Software has three programs denominated as "Scale," "Fringe," and "Difference." Each program has several options to perform various tasks. The program "Scale" provides various image improvement techniques. It is used to extract the magnitude and phase information from the images. The images are first corrected for the so called gamma correction using the program "Scale." An arcsine operation on the square root of normalized image intensity results in the magnitude image. The square root of the normalized intensity distribution is passed through the option "D" in the program "Scale" to obtain the initial phase image. The magnitude and phase images derived from the original image in figure 3.2 are shown in figure 3.3 and figure 3.4

respectively. The magnitude image essentially looks like the original image with a better contrast between dark and bright fringes. The initial phase image shows the edges of fringe bands more prominently. It is passed through a filter to obtain sharp fringe edge lines. An external image editing program "XV" is used to remove the noise in the phase image. Each edge line on the phase image is assigned an integer pixel value which designates the fringe order of the fringe in the region.

The "Expandblack" option in the program "Fringe" is utilized to expand these few assigned pixels to all across each edge line. The option "Displacement" in the program "Fringe" is used to expand the fringe edges to the surrounding regions. In this process the Fringe Analysis Software looks at the corresponding magnitude image to decide if a point falls on one fringe band or the next. Thus, a new phase image is created with less noise, where each point is assigned an integer fringe number as shown in figure 3.5. The fringe order function in this interferogram is not continuous and jumps across the edge lines. It should be noted that this fringe number distribution also represents the out-of-plane deformation field on the domain. The out-of-plane deformation at any point has been rounded off to the nearest integer multiple of the wavelength of light used.

Finally, the program "Difference" is utilized to subtract the images. For this purpose the magnitude and reconstructed phase images of the reference interferogram and any subsequent interferogram are used. The phase and magnitude information of each image is combined to obtain a continuous displacement field and two such displacement fields are subtracted to obtain the desired images.

In the reconstructed phase images and subsequent images, the gray scale value at any pixel point represents the deformation at that point. However, such pixel distribution in a very small range makes it difficult for the human eye to sense the contrast between two regions of different fringe number. To overcome this disability, the following mapping is used to map the images into dark and bright regions.

Gray scale value = (Gray scale value) / 2 + 1, if the fringe number is even.

Gray scale value = (Gray scale value + 255) / 2, if the fringe number is odd.

This function assigns dark pixels (gray scale value < 127) for the even fringe numbers and bright pixels (gray scale value > 127) for the odd fringe numbers. This makes it easier to visualize the fringe patterns. All the reconstructed phase images and subsequent images were created using this nonlinear mapping.

The potential advantage of this Fringe Analysis technique is that it takes into account the actual intensity distribution created by Twyman-Green interferometric technique as given in equation 3.3. Hence the interpolation function between two fringes is a sine-squared function decided by the actual intensity distribution. However, the results obtained using this technique in our investigation were not satisfactory. Figure 3.6 shows the final subtracted image at 55 μs. The resulting image is very noisy. This can be attributed to two main reasons. The images obtained in this experiment have very few fringes. The number of fringes in the reference image is comparable to the number of fringes observed in the subsequent images, so that the noise-to-signal ratio is very high. Secondly, the software has an inherent functional error that leads to erroneous results. A comparison of the recreated phase fringe pattern with the original image (figure 3.5 and figure 3.2) shows that the reconstructed phase configuration has a nearly 90° phase shift compared to the original image. This means the edges of the fringes in the original image correspond to the centers of fringe bands in the reconstructed image. The phase shift between the magnitude and the phase images leads to an erroneous displacement field when the program "Difference" reconstructs the field using the two images. This error in the software did not have much consequence in the earlier studies of crack propagation in PMMA because of high fringe density in the images obtained. However, in the current investigation, only a few fringes are contained in the images and a high noise to signal ratio is superimposed. This flaw in the software leads to erroneous results for the image analysis in the present investigation.

3.3 Image Analysis Procedure

In the previous section it was mentioned that the "Fringe Analysis Software" did not yield satisfactory results in the analysis of interferograms obtained in this investigation. A new "Image Analysis Procedure" is developed to perform the image analysis, which utilizes a fringe edge detection algorithm and the commercial software "MATLAB" to subtract the reference image from subsequent images with little compromise in the accuracy of the results. Instead of using a sine-squared interpolating function between fringes, which is the ideal choice for interferometric techniques, a bilinear cubic function available in the software "MATLAB" is employed.

A new set of experiments were conducted with minor modification in the experimental set-up to be able to utilize the more powerful features of a new pulsed laser that was added to the existing GALCIT facilities. Figure 3.7 shows a typical reference image obtained in these experiments. The images obtained from the experiments are scanned using an *H-P* desk scanner. A window is chosen in each image, which represent the same region on the specimen. A fringe edge detection algorithm is utilized to find the distinct edges of the fringes otherwise not distinguishable to the human eye. Figure 3.8 shows the clearly visible edge lines of the fringe bands in the reference image. The images are digitized using a desktop digitizer. The digitizer provides the x and y coordinates of points on the fringe edge lines and allows to assign fringe numbers to these points. The numbering is conducted starting from 0.25, with increments of 0.5 for each edge, in the ascending or descending order as needed. This is in compliance with the convention that the centers of white fringes are assigned integer fringe numbers. These fringe numbers multiplied by half the wavelength of light used in the experiment give the actual out-of-plane deformation at these points. Care is taken to avoid any discontinuity in the deformation or slope field, which is physically not reasonable.

Around 700 data points are taken for each image using the digitizer. These data points are first checked with the commercial software "Tecplot" to ensure that they represent the images accurately. Tecplot draws a polynomial fit curve through each set of points

having the same fringe order. The result obtained from Tecplot (figure 3.9) matches exactly with the original image. Thus a cubic polynomial fit through these nearly 700 data points provides a very accurate reproduction of the original image.

This raw image data is processed by the commercial software "MATLAB" for further analysis. The "griddata" function in "MATLAB" interpolates the deformation field at these nearly 700 randomly distributed points onto a uniform grid with a given number of points, using a bilinear cubic interpolation function. For this study a uniform grid with 50 nodal points on each axis is chosen. Once all the images are interpolated onto the same grid, the reference image is subtracted from the subsequent images giving the actual deformation values at these finite number of grid points.

Figures 3.10 through 3.27 show contour plots of the subtracted images obtained using the described procedure at 4 μs interval each. The contours in these plots represent constant out-of-plane deformation lines in the deformation field at 0.5 fringe order interval. The x and y coordinate scale shows the actual dimension of the field of view on the specimen.

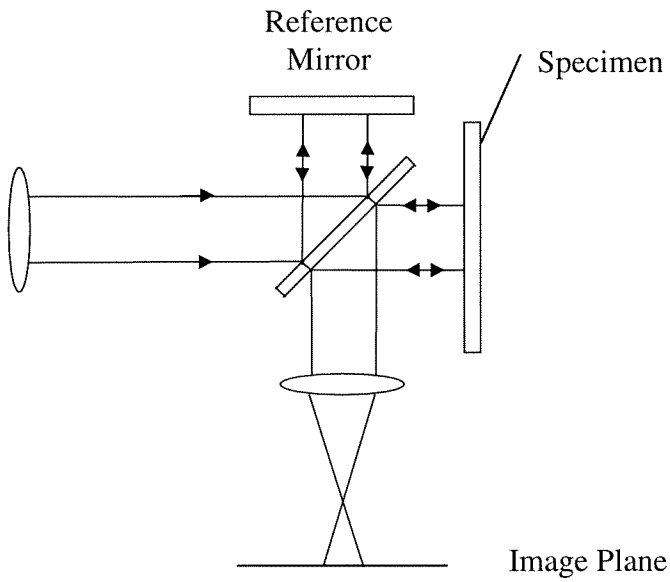

Figure 3.1 : Schematic diagram of Twyman-Green interferometer.

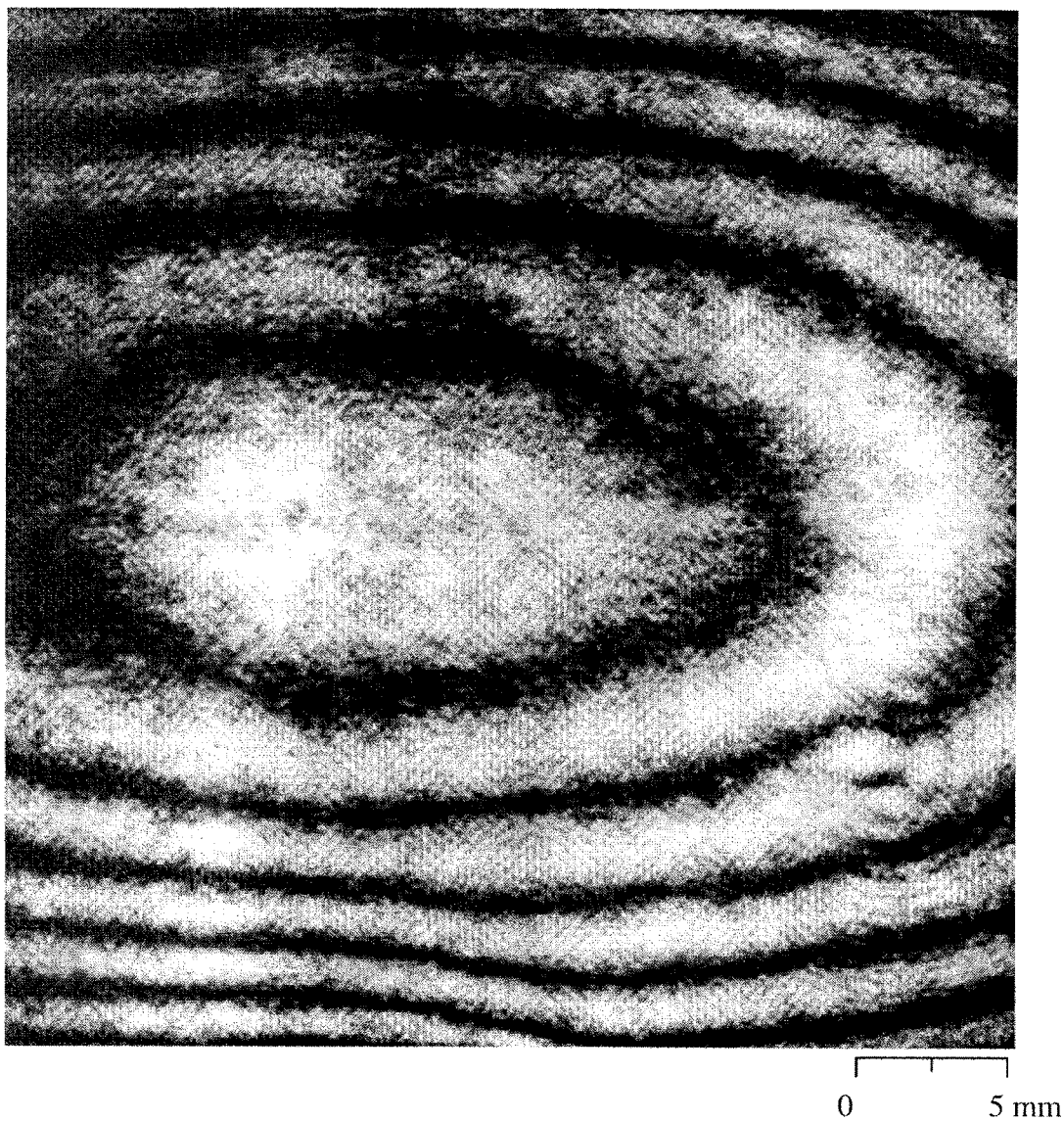

Figure 3.2 : Reference image.

Figure 3.3 : Magnitude image of the reference image.

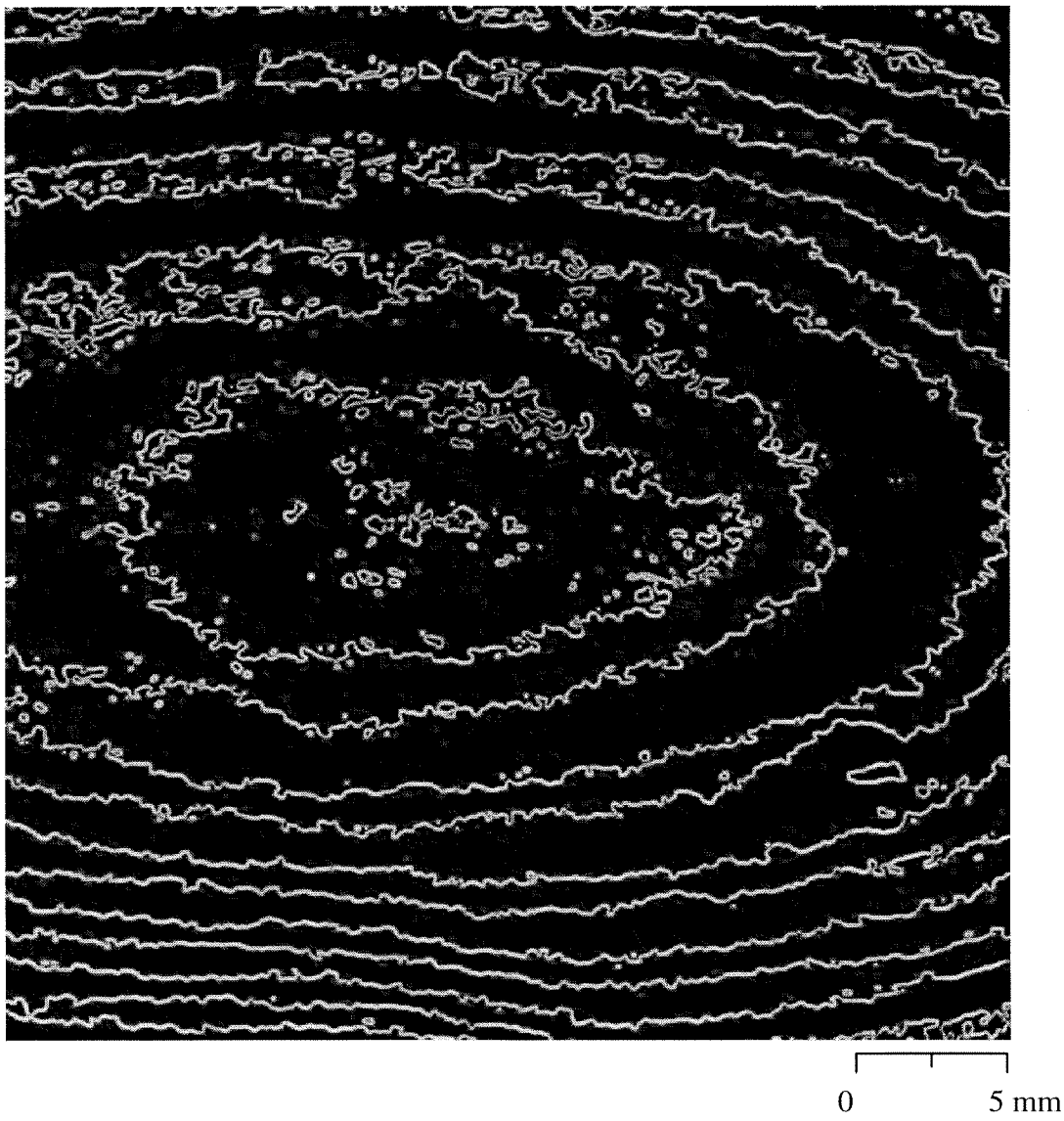

Figure 3.4 : Initial phase image of the reference image.

Figure 3.5 : Reconstructed reference phase image.

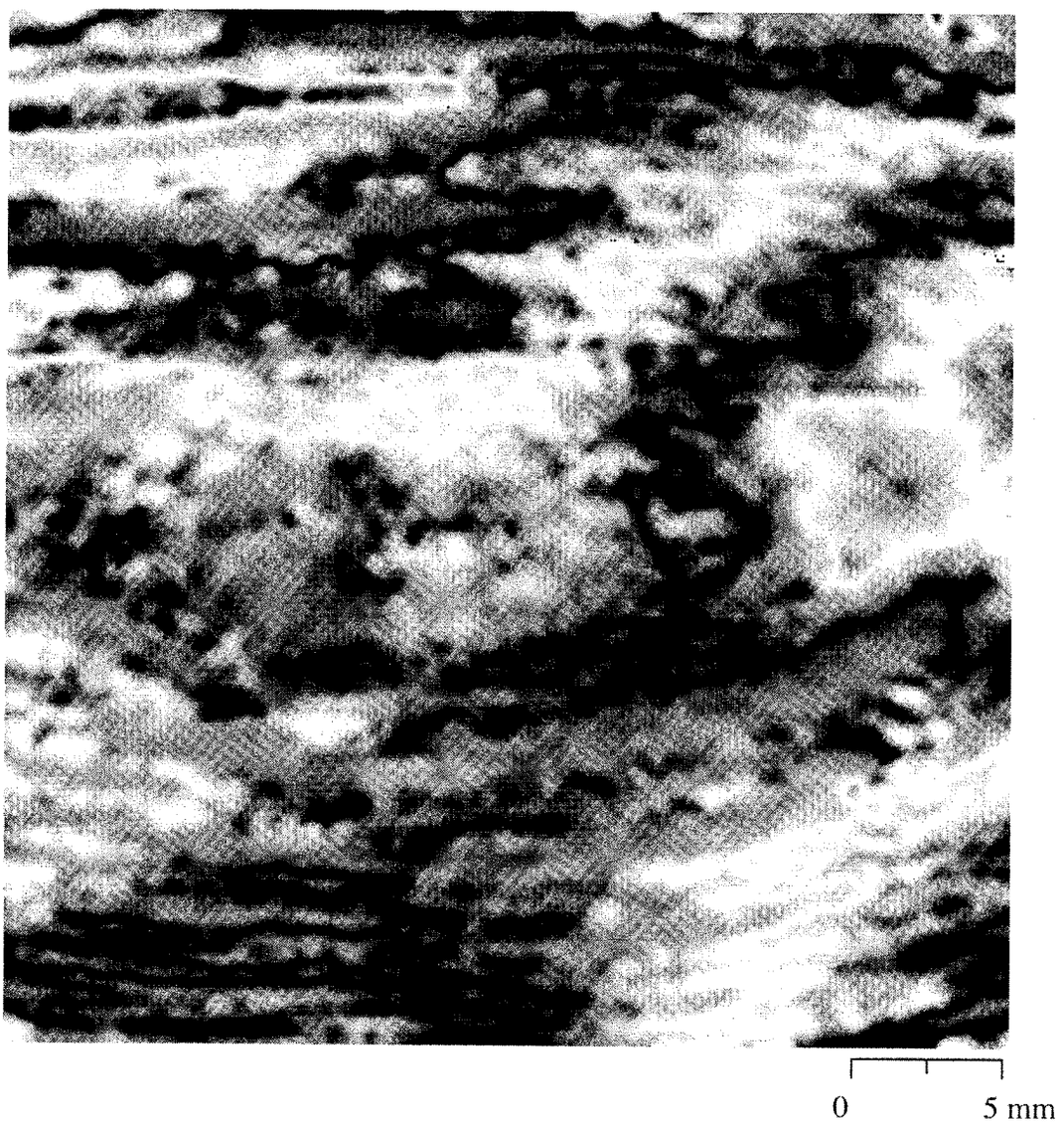

Figure 3.6 : Difference between image at 55 μs and the reference image.

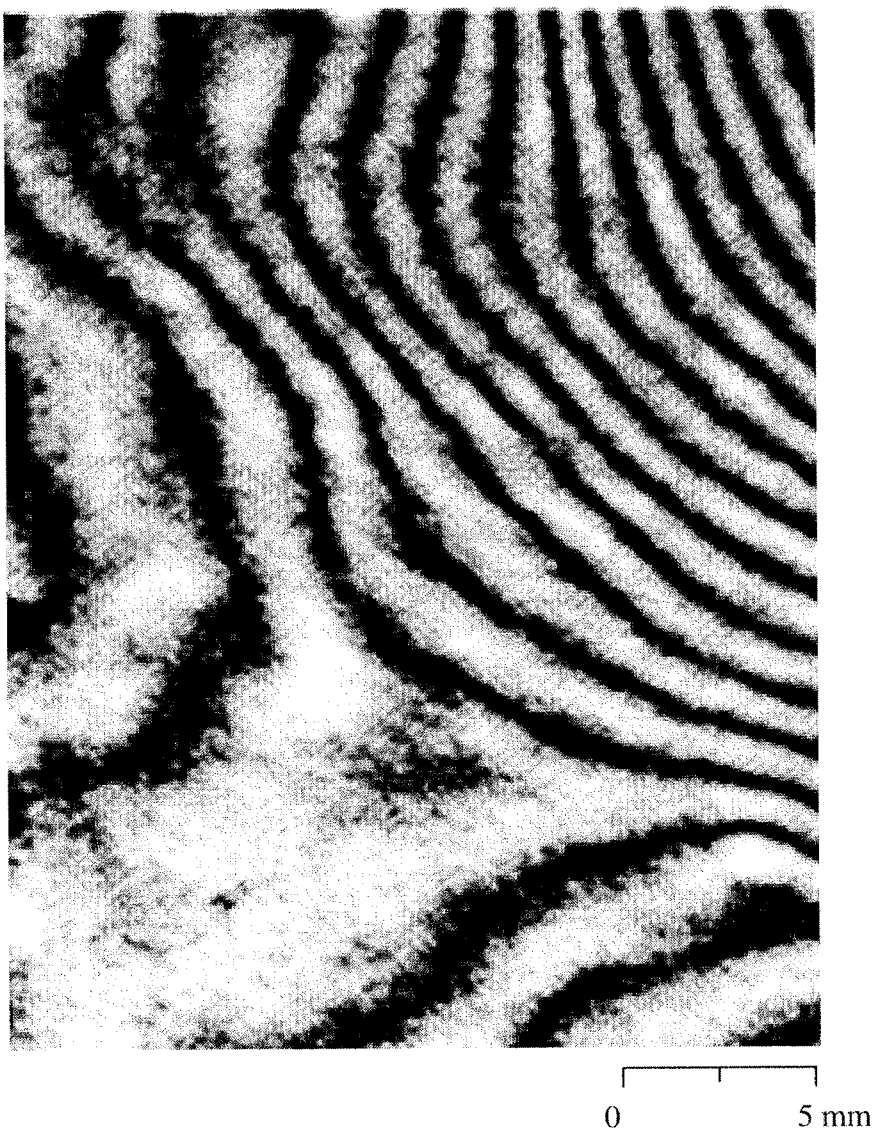

Figure 3.7 : Reference image from a new set of experiments.

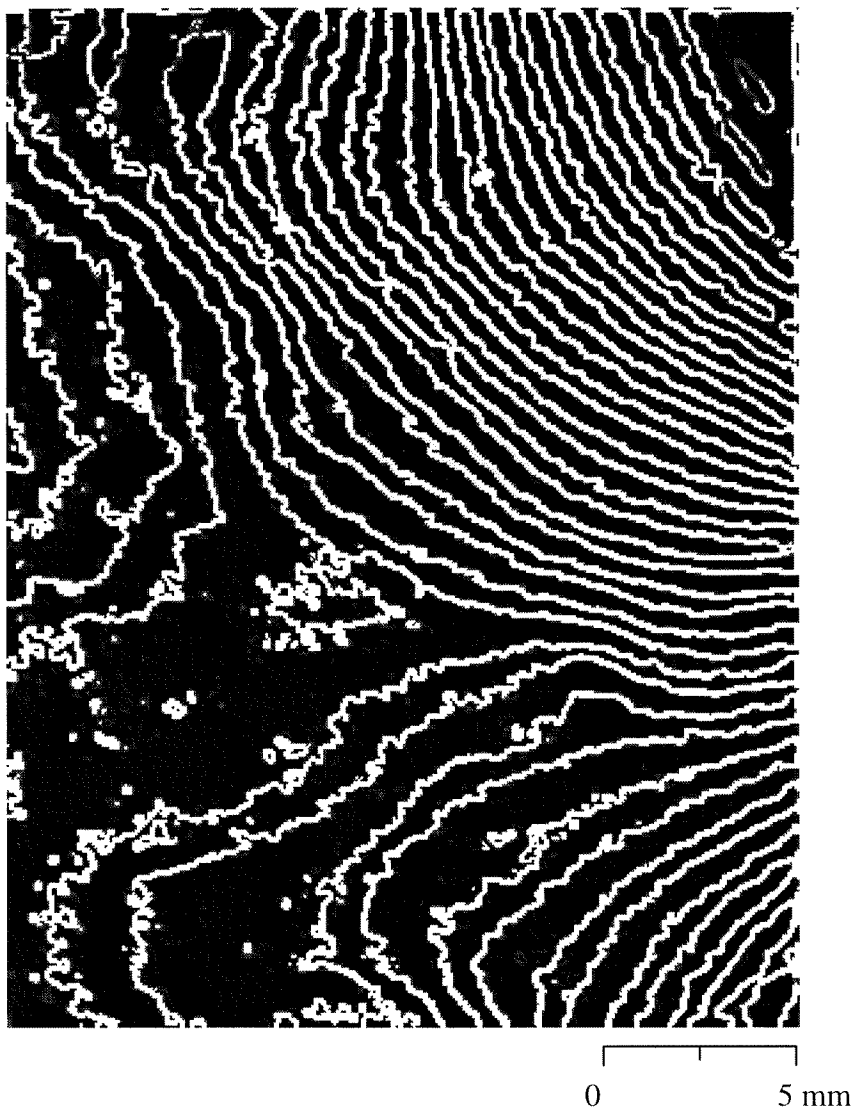

Figure 3.8 : Fringe edge lines in the reference image.

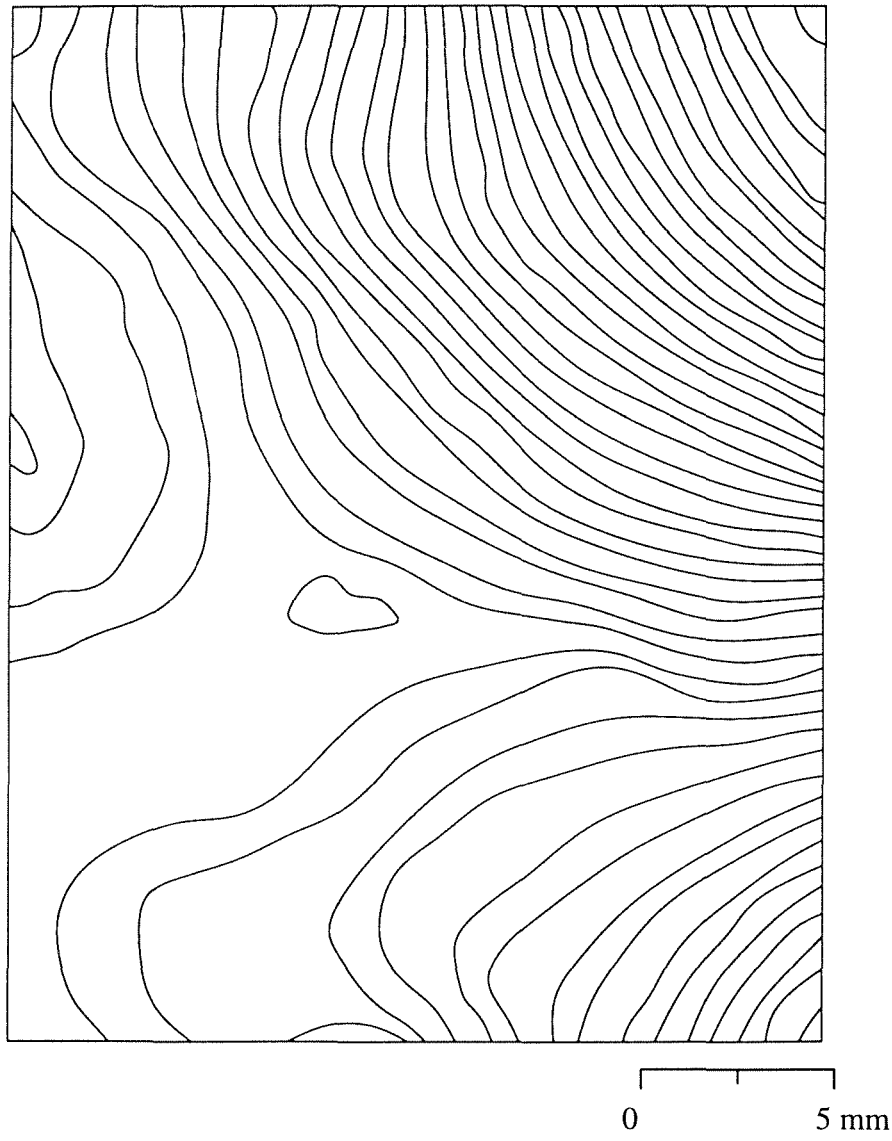

Figure 3.9 : Reconstructed reference image using the spline interpolating function in Tecplot.

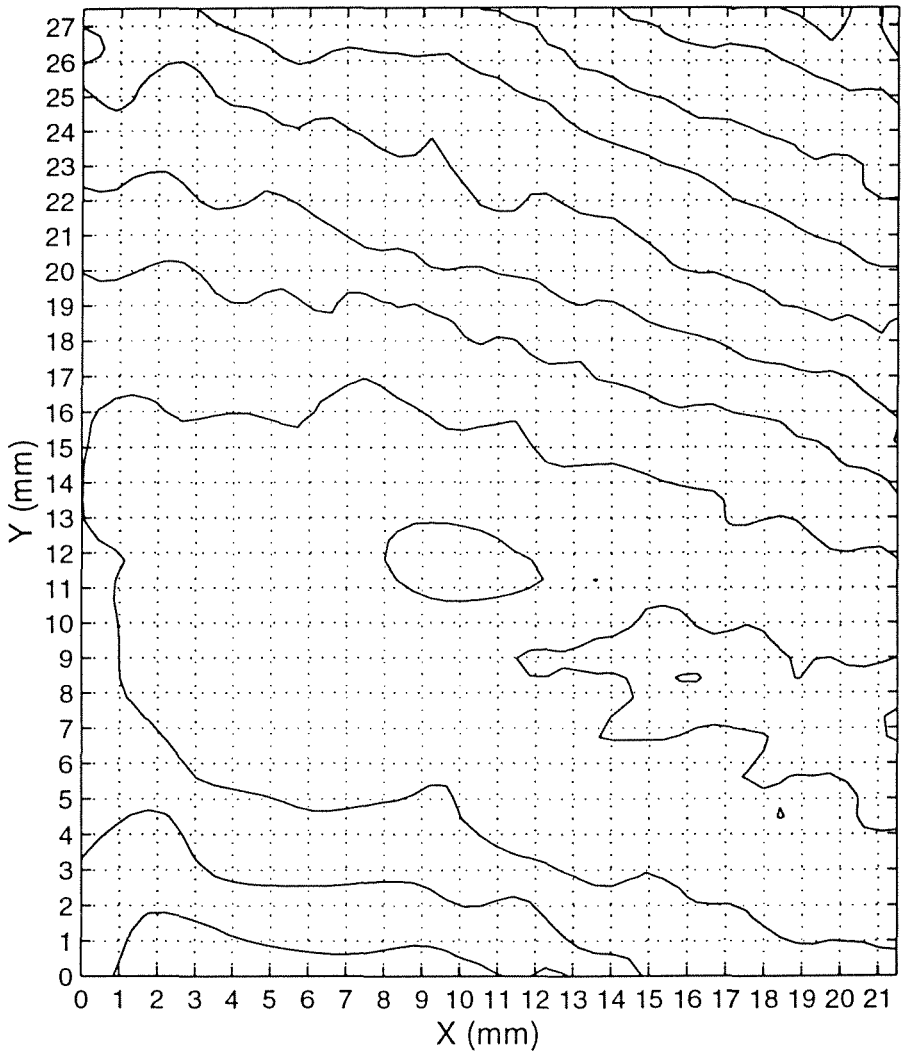

Figure 3.10 : Contour plot of the difference image at 0 μs.

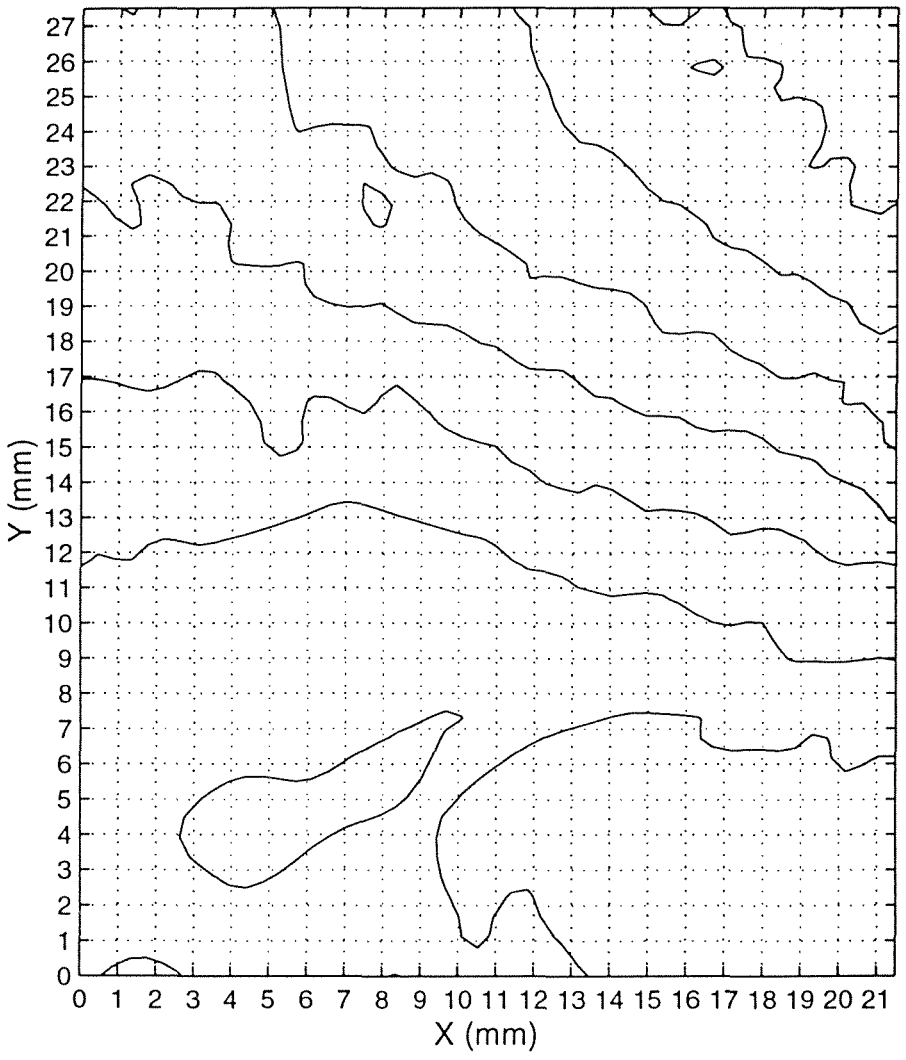

Figure 3.11 : Contour plot of the difference image at 4 μs.

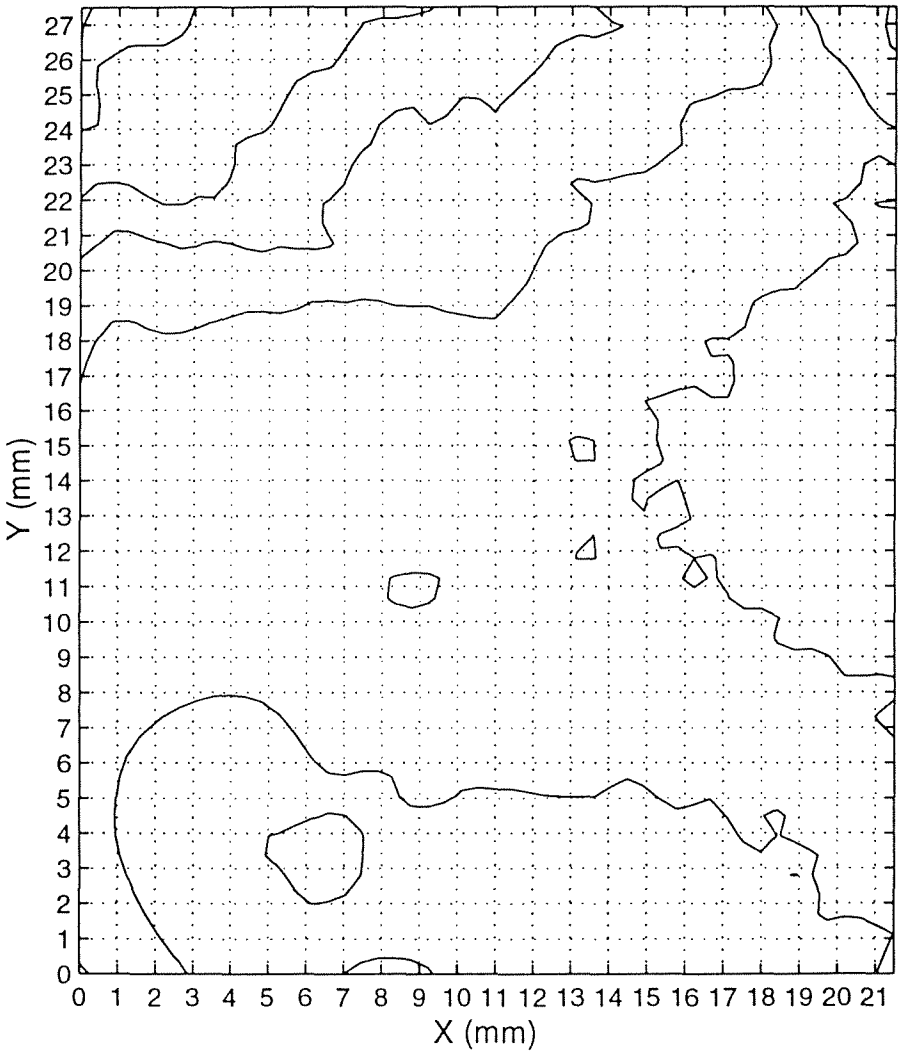

Figure 3.12 : Contour plot of the difference image at 8 μs.

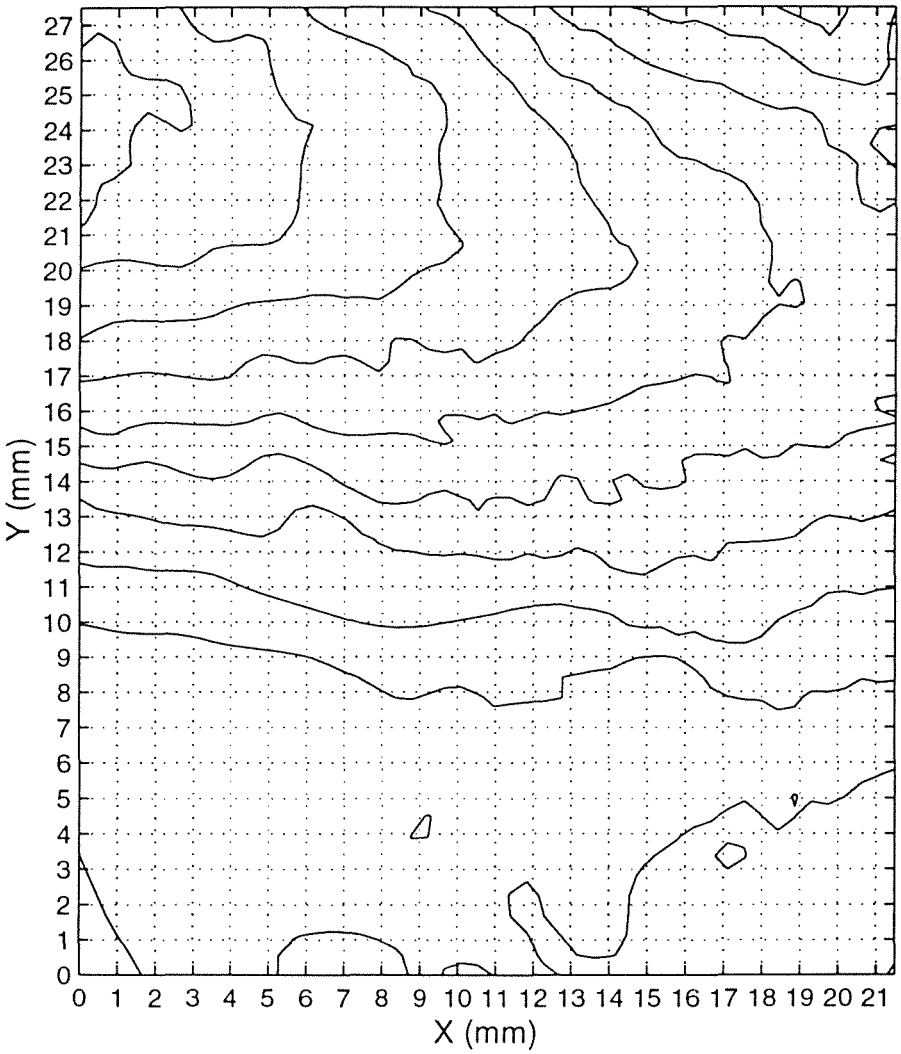

Figure 3.13 : Contour plot of the difference image at 12 μs.

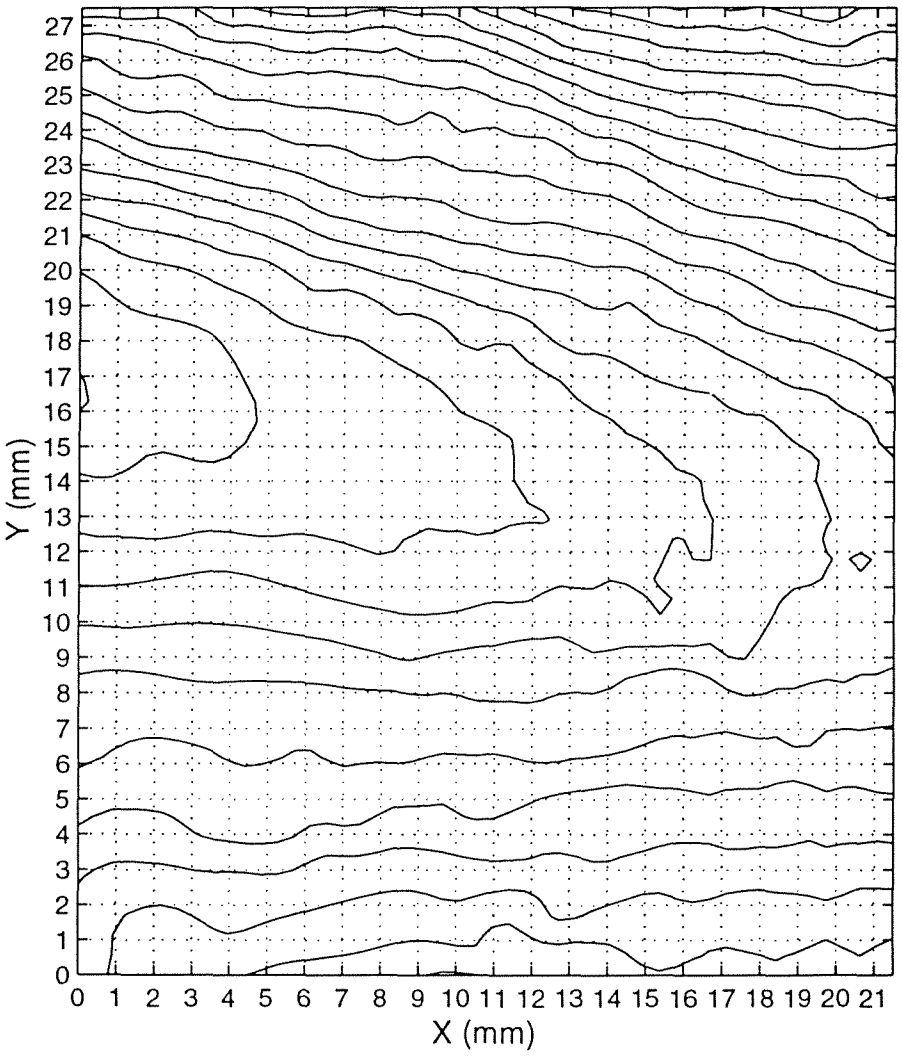

Figure 3.14 : Contour plot of the difference image at 16 μs.

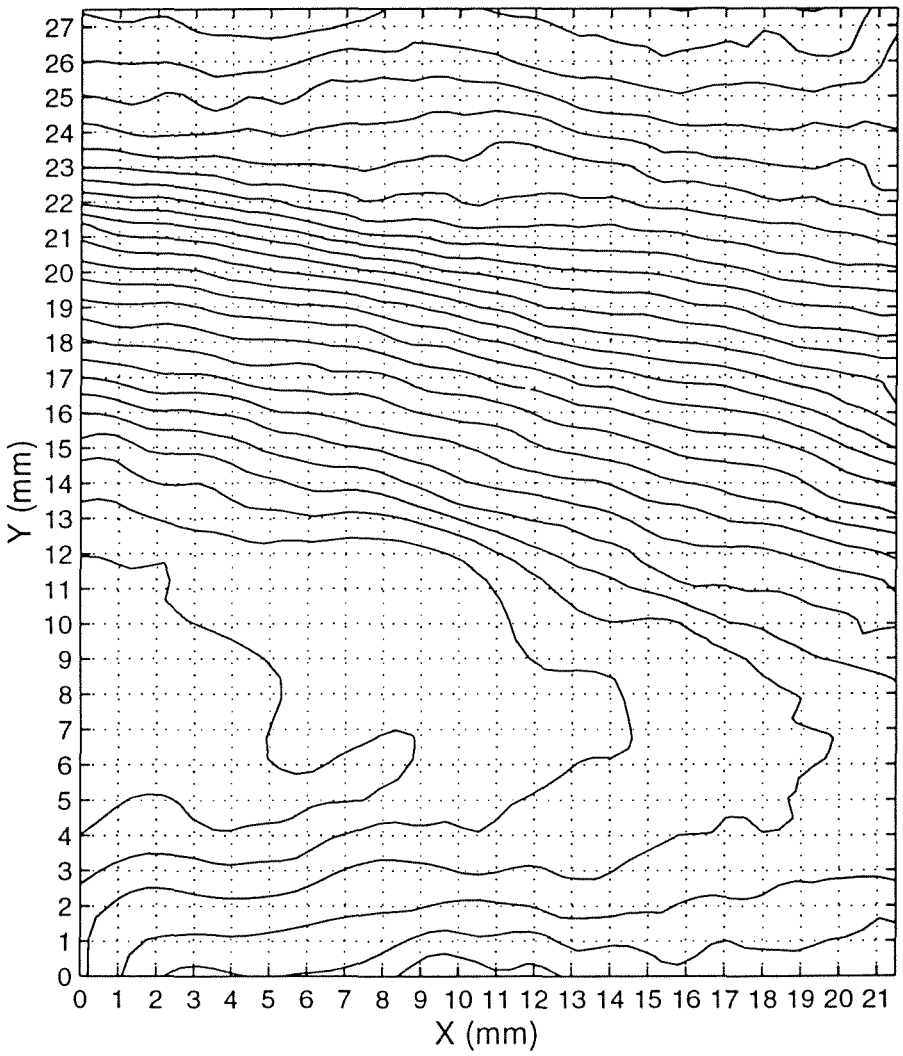

Figure 3.15 : Contour plot of the difference image at 20 μs.

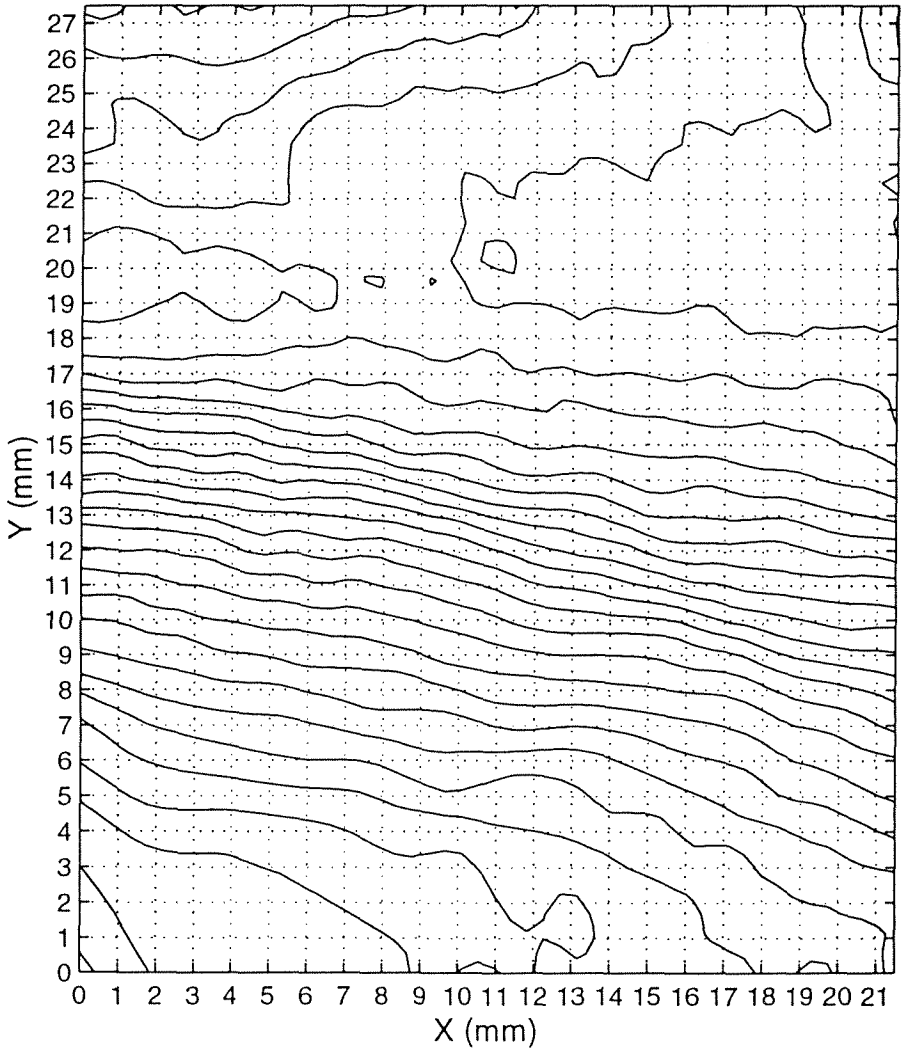

Figure 3.16 : Contour plot of the difference image at 24 μs.

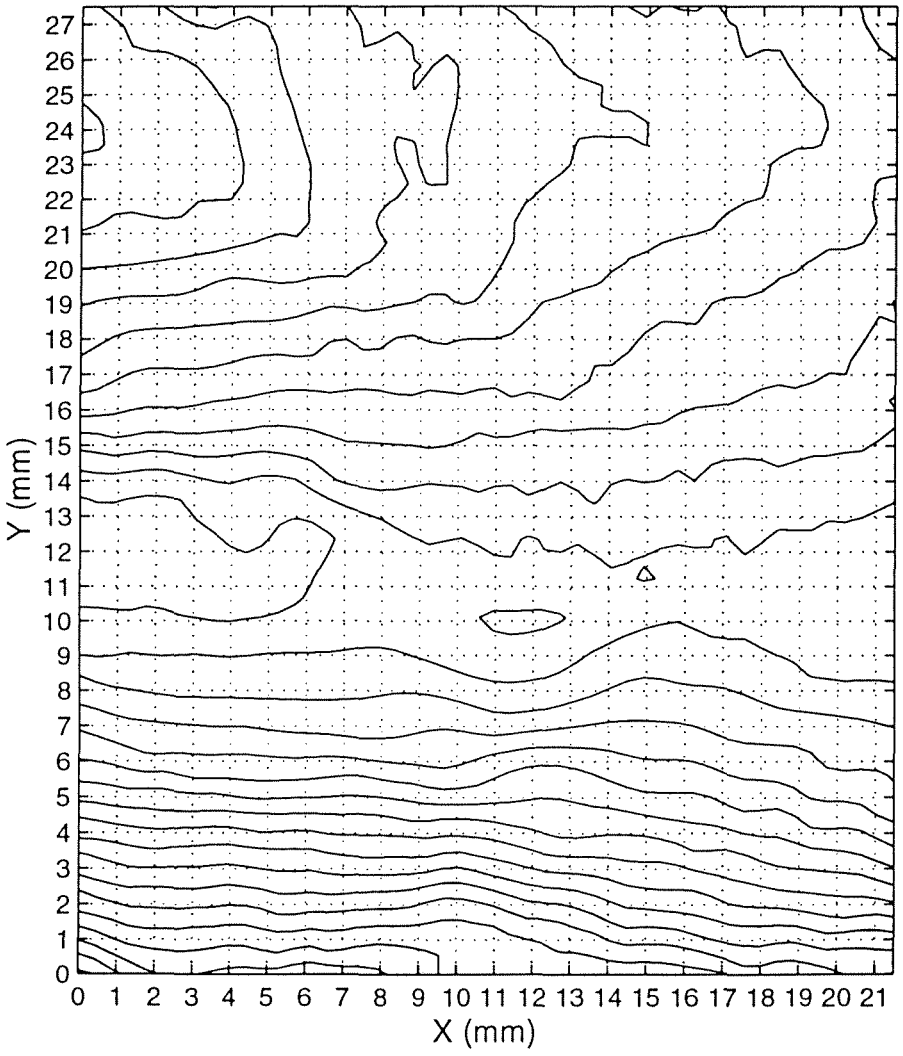

Figure 3.17 : Contour plot of the difference image at 28 μs.

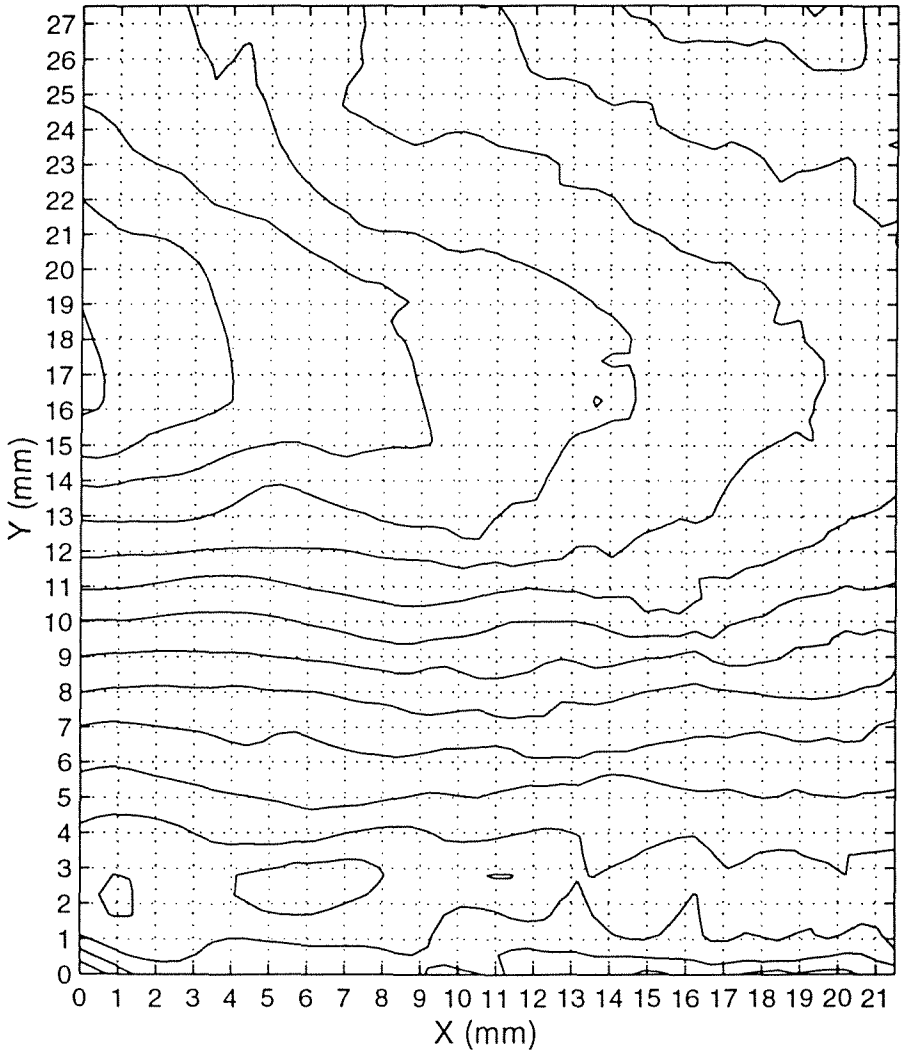

Figure 3.18 : Contour plot of the difference image at 32 μs.

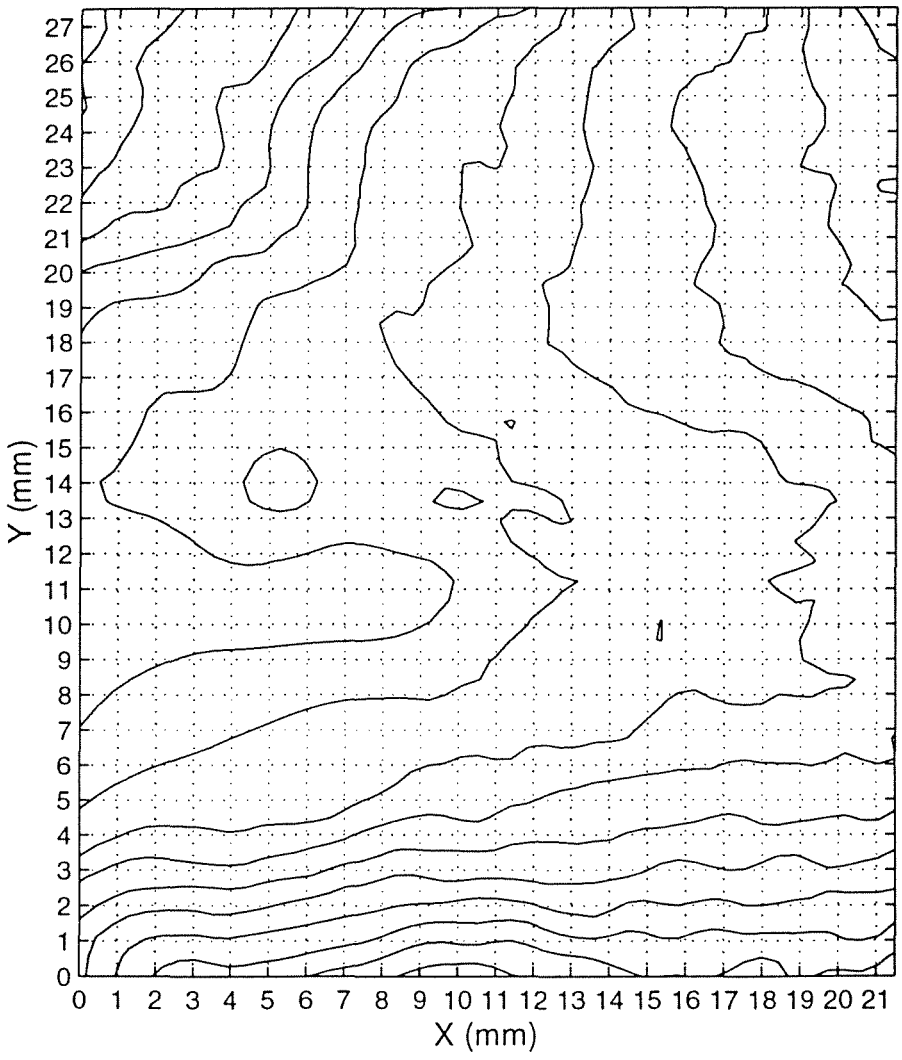

Figure 3.19 : Contour plot of the difference image at 36 μs.

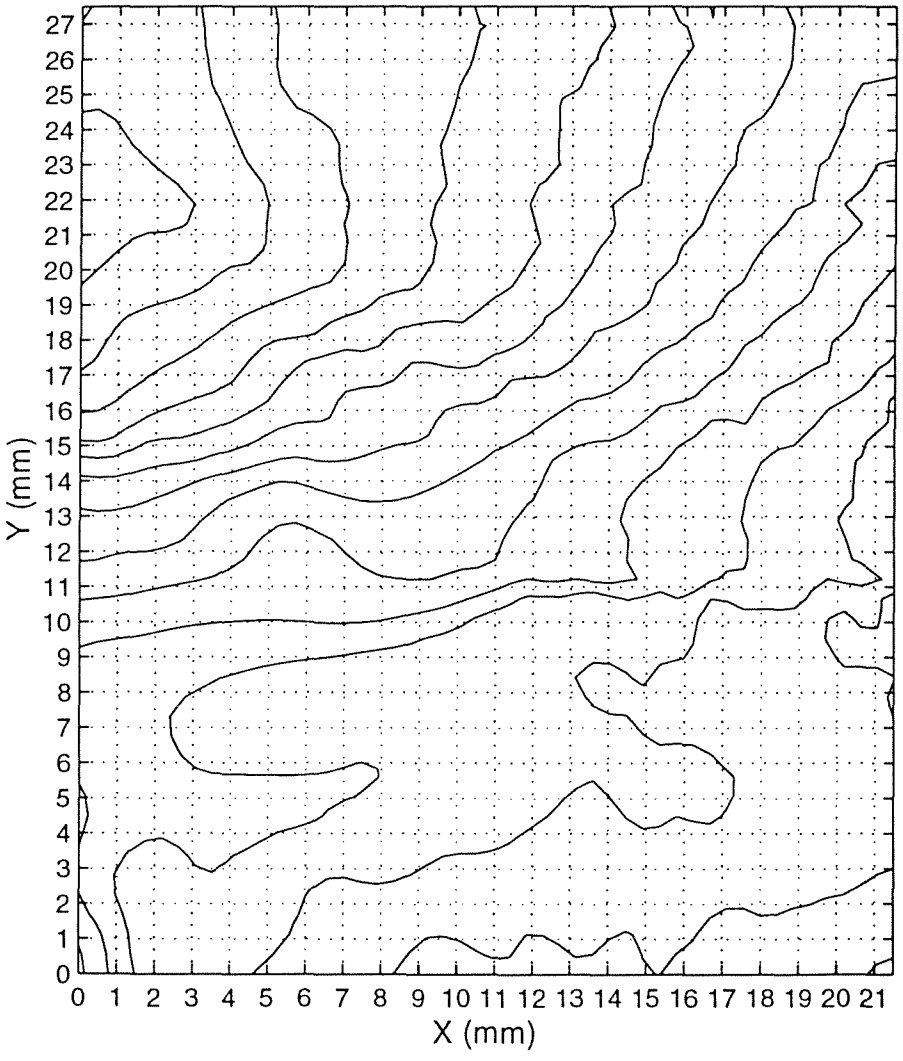

Figure 3.20 : Contour plot of the difference image at 40 μs.

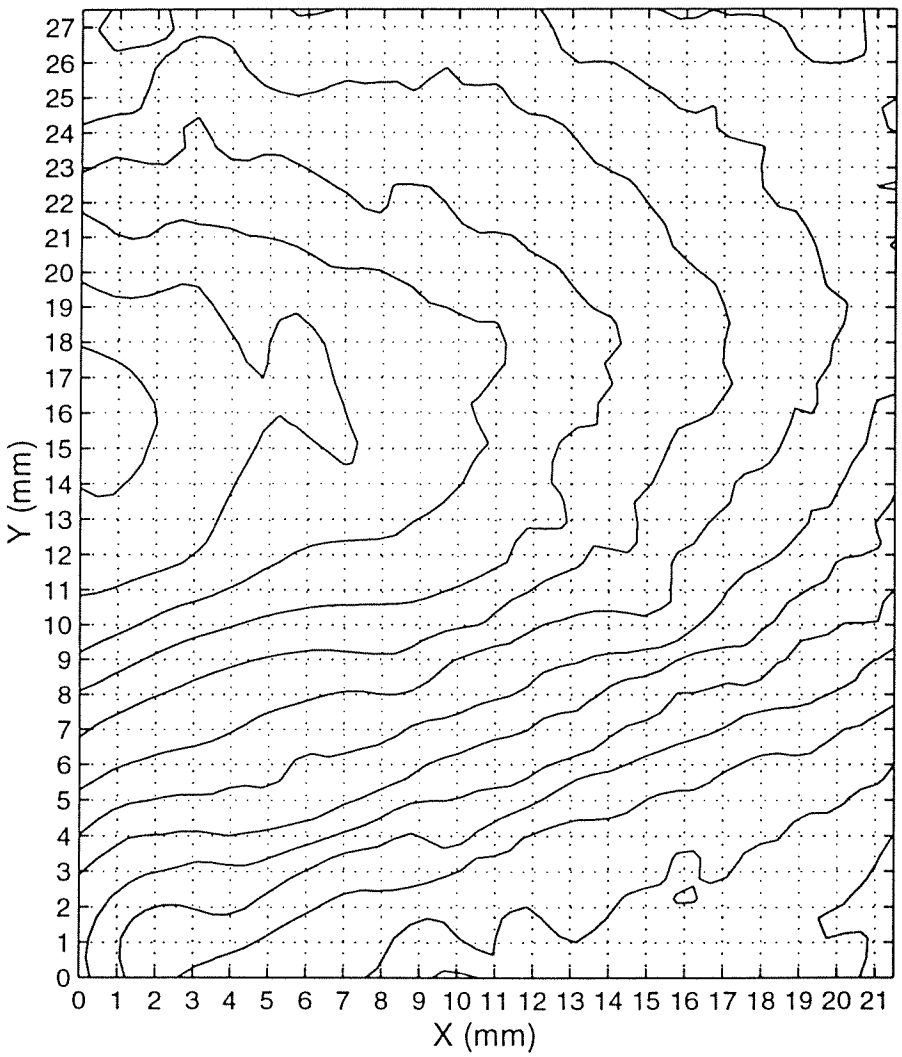

Figure 3.21 : Contour plot of the difference image at 44 μs.

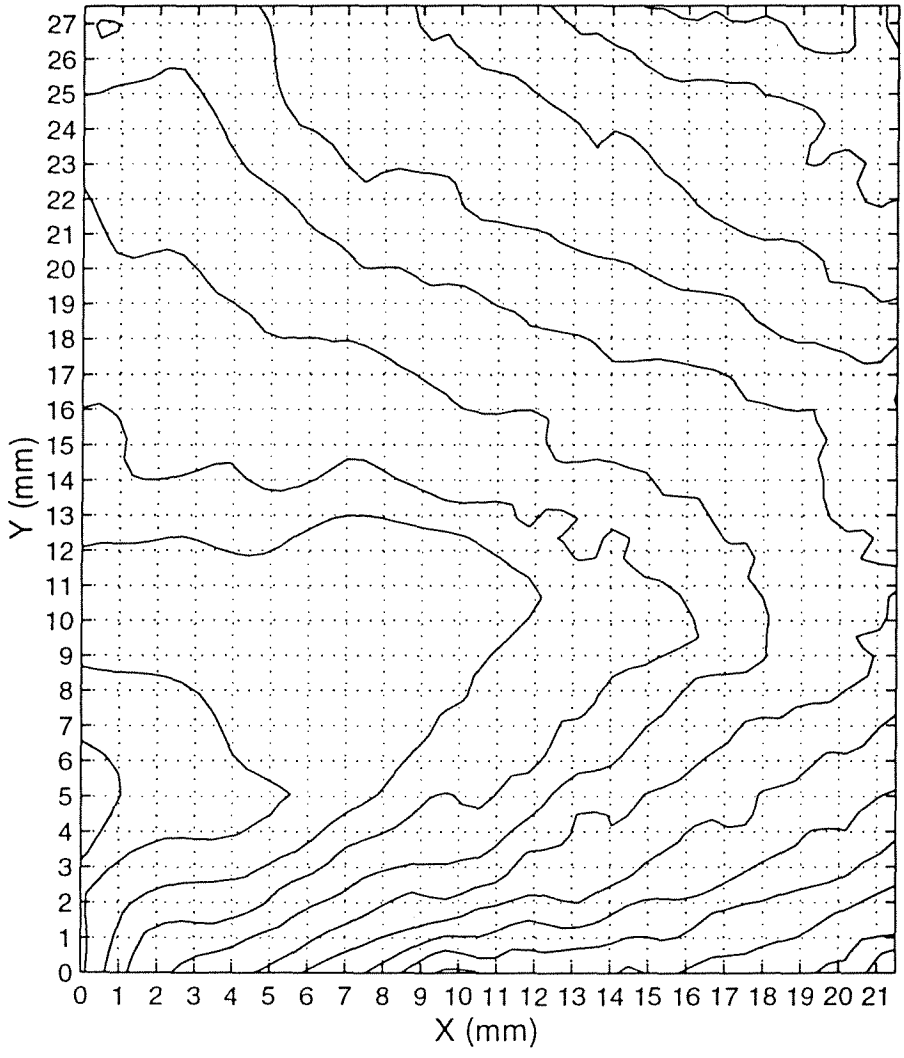

Figure 3.22 : Contour plot of the difference image at 48 μs.

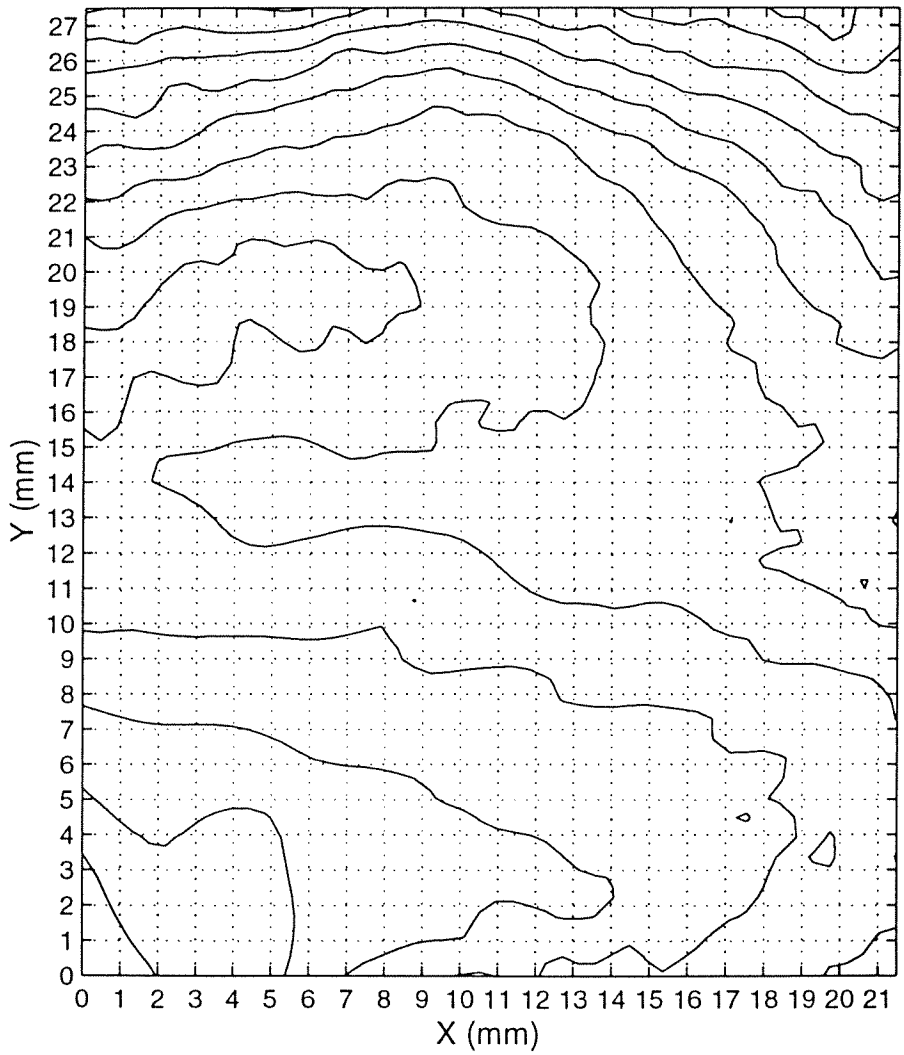

Figure 3.23 : Contour plot of the difference image at 52 μs.

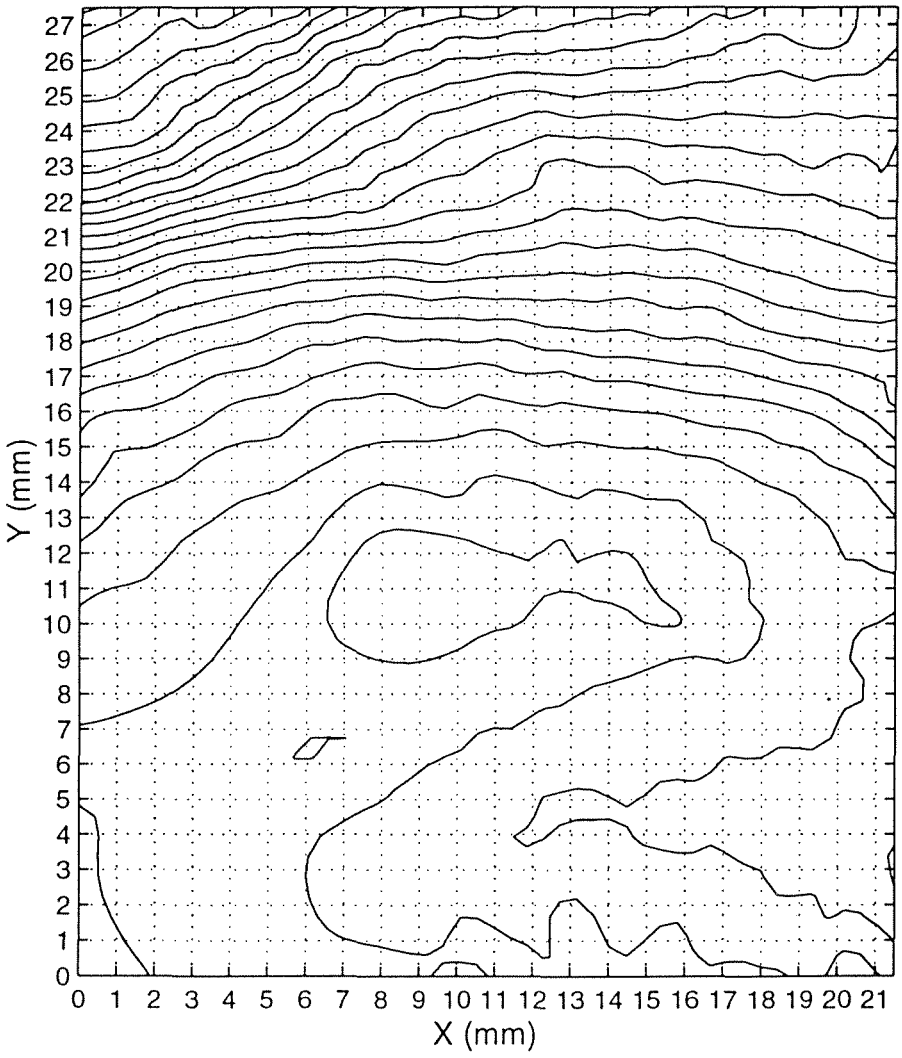

Figure 3.24 : Contour plot of the difference image at 56 μs.

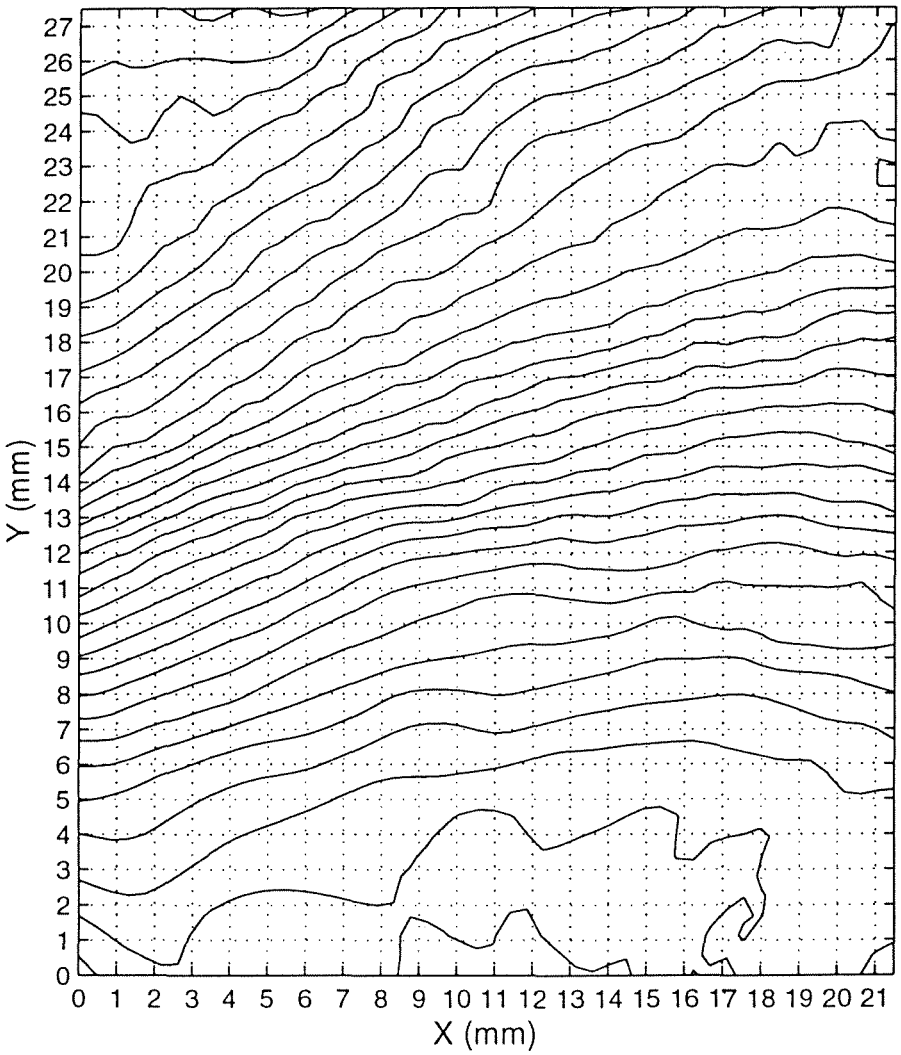

Figure 3.25 : Contour plot of the difference image at 60 μs.

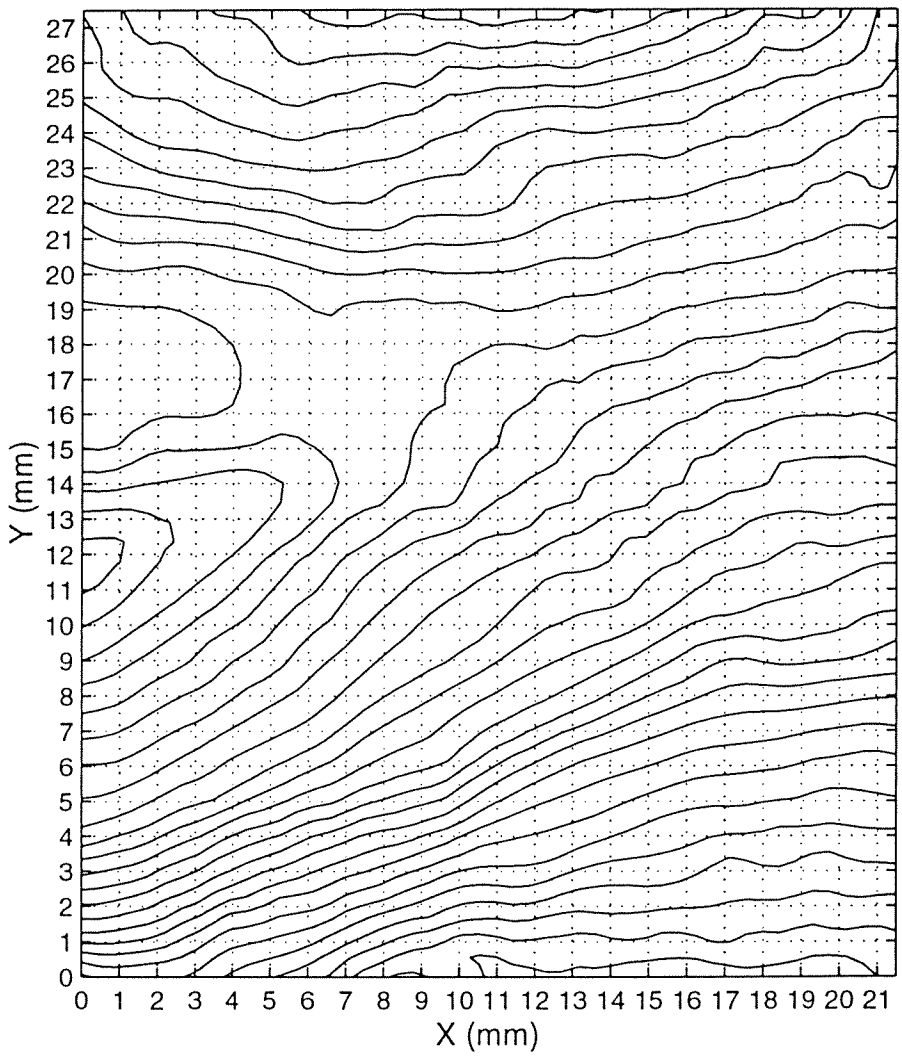

Figure 3.26 : Contour plot of the difference image at 64 μs.

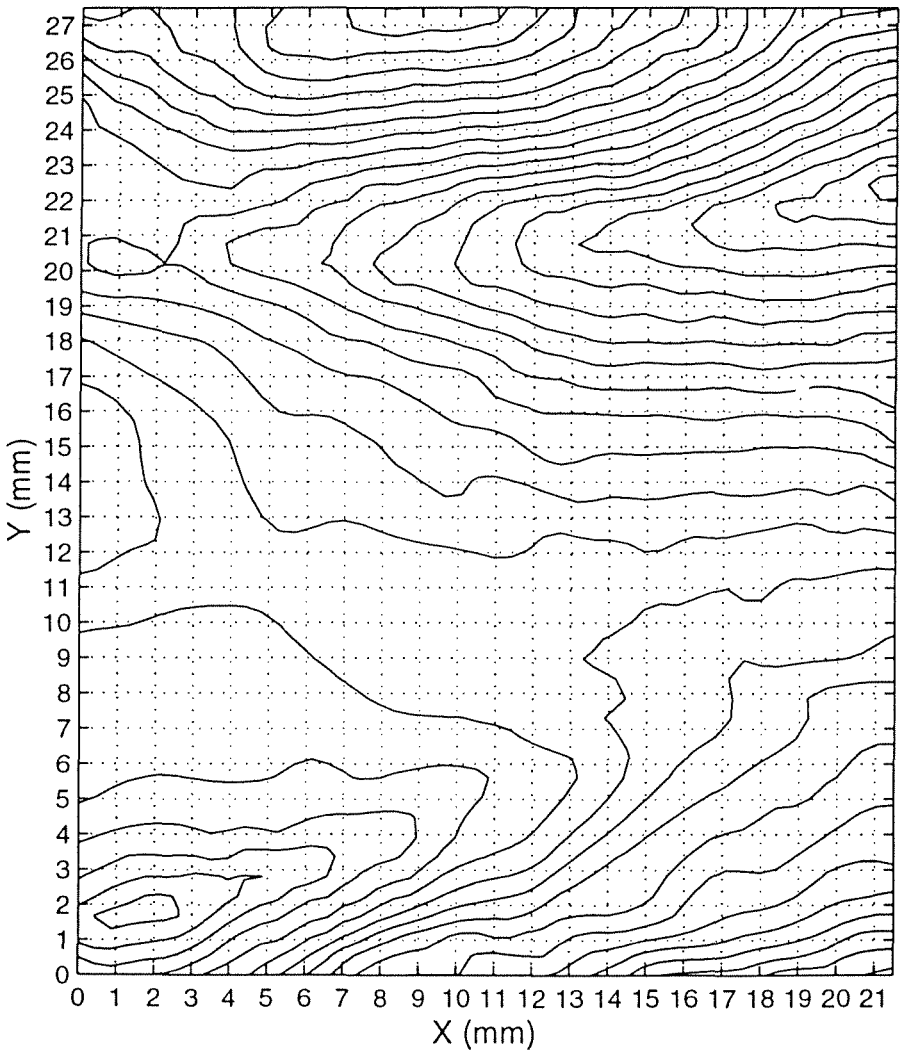

Figure 3.27 : Contour plot of the difference image at 68 μs.

4. Results and Discussion

In the previous chapter, a new image analysis method is described that employs a fringe edge detection algorithm and the commercial software "MATLAB" to subtract the reference image from subsequent images. Figures 3.10 through 3.27 show the images obtained using this method. These interferograms show the actual fringe distribution created by propagating stress waves at 4 μs intervals. A comparison of two successive images, for example figure 3.17 at 28μs and figure 3.18 at 32 μs, reveal that the fringe pattern in these images travel "downward" in the specimen with time. However, it is difficult to clearly identify the same features in consecutive images accurately to obtain the speed and magnitude of the wave propagation because the two-dimensional fringe features change in shape as they move. For this reason a comparatively small vertical strip is chosen to observe the propagation of waves. The strip is 11 points wide in the x direction (20% of the image width) at the center of the horizontal axis. The mean value of the out-of-plane deformation values at 11 points along any horizontal line is taken as the deformation at that y coordinate. This averaging procedure maps the deformation field onto a one-dimensional plot, which makes the quantitative measurement much easier and minimizes the effect of local disturbances.

Comparing the one-dimensional deformation field patterns, the downward propagating features are identified more accurately in successive images. The travel of identifiable features (peaks and valleys) in successive images can be measured which provides the distance traveled by the stress pulse during the inter-frame time (4 μs). Thus the speed of the stress wave in each frame is obtained and is plotted against time in figure 4.1. The plot shows an average wave velocity of 2000 m/s. As the distance traveled by the stress pulse between any two frames is known, one can shift the frames by that distance along the vertical direction to obtain a profile of the out-of-plane deformation. Figure 4.2 shows the deformation profile over 167.8 mm on the specimen surface. The field of view on the specimen is located 150 mm from the top edge of the specimen where the

stress wave was imparted. Assuming an average wave speed of 2000 m/s, the wave completely occupies the 27.5 mm tall field of view approximately 88 μs after the electromagnetic force generator is triggered. The first interferogram (referred to as the image at 0 μs in figure 3.10) is created by the leading 27.5 mm of the deformation profile shown in figure 4.2.

The out-of-plane deformation on the specimen surface is created by the in-plane stress wave as well as the flexural wave. When the copper strips are forced apart by the electromagnetic pressure field generated by the current flowing through the strips, the lower leg of the conductor imparts the plate stress on the specimen. If the copper strips are not perfectly aligned with the center of the top edge of the specimen, they also cause a net bending moment on the specimen. The bending moment, though small in magnitude, produces a comparatively large surface deformation due to the low bending moment of inertia of the specimen while the out-of-plane deformation on the specimen surface generated by the in-plane plate stress wave is through Poisson's effect and is small in magnitude.

4.1 Estimation of Deformation Generated

In the following section a comparison of out-of-plane deformations generated by an in-plane stress wave and a flexural wave are estimated and compared for a statically loaded plate.

Deformation due to in-plane stress wave

For a plane stress loading, the strain in z-direction (see figure 4.3) produced by a uniaxial stress field is expressed as

$$\varepsilon_{yy} = -\frac{\nu}{E}\sigma_{yy} \tag{4.1}$$

where

ε_{yy} : Longitudinal strain in y direction

σ_{yy} : Stress in y direction

ν : Poisson's ratio

E : Elastic modulus of elasticity.

The magnitude of the out-of-plane deformation on the specimen surface is derived by integrating the expression in equation 4.1 along the thickness of the specimen. Due to symmetry, the deformation is zero at the center of the thickness. Equation 4.1 reduces to

$$w = \frac{\nu t \sigma_{yy}}{2E} \tag{4.2}$$

where

w : Out-of-plane deformation on the specimen surface

t : Thickness of the specimen.

So, the fringe order (f) obtained at any point due to the plate stress takes the form

$$f = \frac{\nu t}{E\lambda}\sigma_{yy}. \tag{4.3}$$

Upon substituting the material properties of Break-Away glass (ν = 0.34 and E = 3.88 GPa), the thickness of the specimen (t = 6.4 mm) and the wavelength of light used in the experiment (λ = 514 nm), the relation between the fringe order (f) and the magnitude of plate stress (σ_{yy}) applied on the specimen in this investigation simplifies to

$$f = 1.1\ \sigma_{yy}, \tag{4.4}$$

where σ_{yy} is measured in MPa.

The peak stress applied on the specimen in this experiment is 0.86 MPa. Therefore, the maximum fringe order produced by the propagating plate stress wave is 0.94.

Estimation of Deformation generated by flexural waves

The plate stress wave imparted on the top edge of the specimen can also produce a net bending moment on the specimen due to any eccentricity in loading. If the stress applied on the top edge of the specimen is off-set from the line of symmetry by 10% of the thickness of the specimen, the peak bending moment exerted per unit width is 3.52 N (stress = 0.86 MPa, thickness = 6.4 mm, eccentricity = 0.64 mm). The bending moment of inertia per unit width of the specimen on the x-z plane is 84.8 Nm (thickness = 6.4 mm, Modulus of elasticity = 3.88 GPa). So, the maximum curvature applied at this edge of the specimen is

$$\frac{d^2w}{dx^2} = 0.042 \text{ m}^{-1} \tag{4.5}$$

To obtain an approximate estimation of the out-of-plane deformation created by this initial curvature, let us consider the region represented by quarter a wavelength of the leading wave in the stress profile. Under the assumption that the initial curvature imparted to the specimen remains a constant over this 10 mm region and the initial displacement (w) and slope (dw/dx) are zero, the maximum out-of-plane deformation is estimated to be 4.2 μm. This deformation would create a fringe order of 16.3 in the interferograms, as compared to a maximum fringe order of 0.94 created by the in-plane stress wave.

Thus a small misalignment of 0.64 mm in the positioning of the copper strips produces flexural waves, which can generate substantial out-of-plane deformations compared to those created by in-plane stress waves through poison's effect. In the current loading device, it is difficult to achieve alignment to such high precision. The slot in the upper holding block of the loading device is used to position the copper strips and the plate together. The slot has enough clearance to make sure that the copper strips move freely in it and transmit the generated pressure pulse to the specimen without any restraint. The flexural waves generated by this misalignment dominate the deformation profile observed in the experiments in this investigation resulting in oscillatory deformation

profile as seen in figure 4.2. The loading device needs to be further improved to reduce the effect of the flexural waves.

4.2 Summary

Break-Away glass is a brittle material with a low fracture tensile strength. It possesses brittle characteristics, which makes it the ideal choice as a model material to investigate the interaction of waves in cracked ceramic armor media. However, due to its low strength, it poses a challenge to prepare plate specimens to be used in experiments in the laboratory. The usual milling, grinding and cutting process break the specimen into pieces and cannot be used to get an optically flat surface. In this investigation, a method is developed where the specimen is cast in an open steel mold. Mold release agents and Teflon tapes are used to prevent glass adherence to the mold. An optimum cooling process is developed, which prevents thermal stress build-up in the specimen during the cooling process. The procedure, described in detail in the Appendix, yields Break-Away glass plate specimens of 300 $\times$300 mm dimension possessing an optically smooth, but not optically flat surface on one side.

The dynamic experiments employ a Lorentz stress wave generator that provides a pressure pulse; a loading device to impart a pressure pulse to the specimen along one edge; an optical set-up for Twyman-Green interferometry technique that captures the fringe patterns generated by the propagating stress waves using a high speed camera; an electronic circuit to synchronize the triggering of the capacitor bank, the laser and the high speed camera. The upper holding block in the loading device holds the copper strip and the top edge of the specimen together and transfers the pressure pulse generated by the copper strip to the specimen. The alignment of the copper conductor with the upper edge of the specimen is very important. As described in "Results and Discussion," a small eccentricity in the alignment causes a net bending moment on the upper edge of the specimen, which produces surface deformations that are large compared to those created by the in-plane stress waves through poison's effect. The

out-of-plane deformations created by the flexural wave are oscillatory in nature and seem to dominate the fringe patterns observed in this experiment. The loading device in the experimental set-up needs to be further improved to prevent any on-set of flexural waves to be able to isolate the plate stress waves. Also, the number of fringes created by the plate stress waves is very small. This is due to the low strength of the material and a comparatively high modulus of elasticity ($E / \sigma_{max} = 776$). A human error in selecting the same window in all the images obtained in an experiment may result in an error comparable to the number of fringes created by the stress wave in Twyman-Green interferometry. Both Twyman-Green interferometry and Photoelasticity yield low fringe density in the images obtained. Fringe multiplication techniques need to be employed to improve the fringe density in either technique. The experimental set-up for fringe multiplication in photoelasticity is, relatively, simpler compared to that for Twyman-Green interferometry.

Finally, a generalized image analysis method is presented to analyze fringe patterns obtained in optical techniques utilizing interference of light. At present, the fringe analysis process in these techniques remains a tedious and time-consuming process prone to human error in tracing the fringe lines. Several papers in the literature have been devoted to developing fringe-tracing algorithms, but a generalized automatic procedure is yet to be developed. In this investigation, a simple 4-step fringe analysis method is presented, which utilizes the powerful tools available in the commercial software such as "Matlab" and fringe edge detection algorithms developed at GALCIT to obtain the field represented by the interferograms.

1. The images are scanned using a desktop scanner. Several image improvement operations available in various commercial software are performed to reduce the noise in the images.
2. The option "D" in the program "Scale" of the "Fringe Analysis Software" is employed to obtain the fringe edge lines in the interferograms. This operation

eliminates any subjective element introduced by manual fringe tracing as it provides sharp edges of the fringe bands.

3. The points on the fringe edge lines are extracted using a digitizer and assigned fringe numbers.
4. The function "griddata" in "Matlab" is used to interpolate the field values at these randomly distributed points onto the nodes of a user supplied uniform grid. This procedure enables the user to obtain the field value at any point on the domain accurately. In the present investigation, the reference image is subtracted from the subsequent images to get the true deformation field.

Only step 3 in this procedure requires manual operation. This step can be easily automated as the edge lines obtained from the "Fringe Analysis Software" are sharp and distinct. The gray level values at the pixel points on the edge lines are greater than 75 and in the rest of the image are less than 75, which can be readily recognized by a computer algorithm.

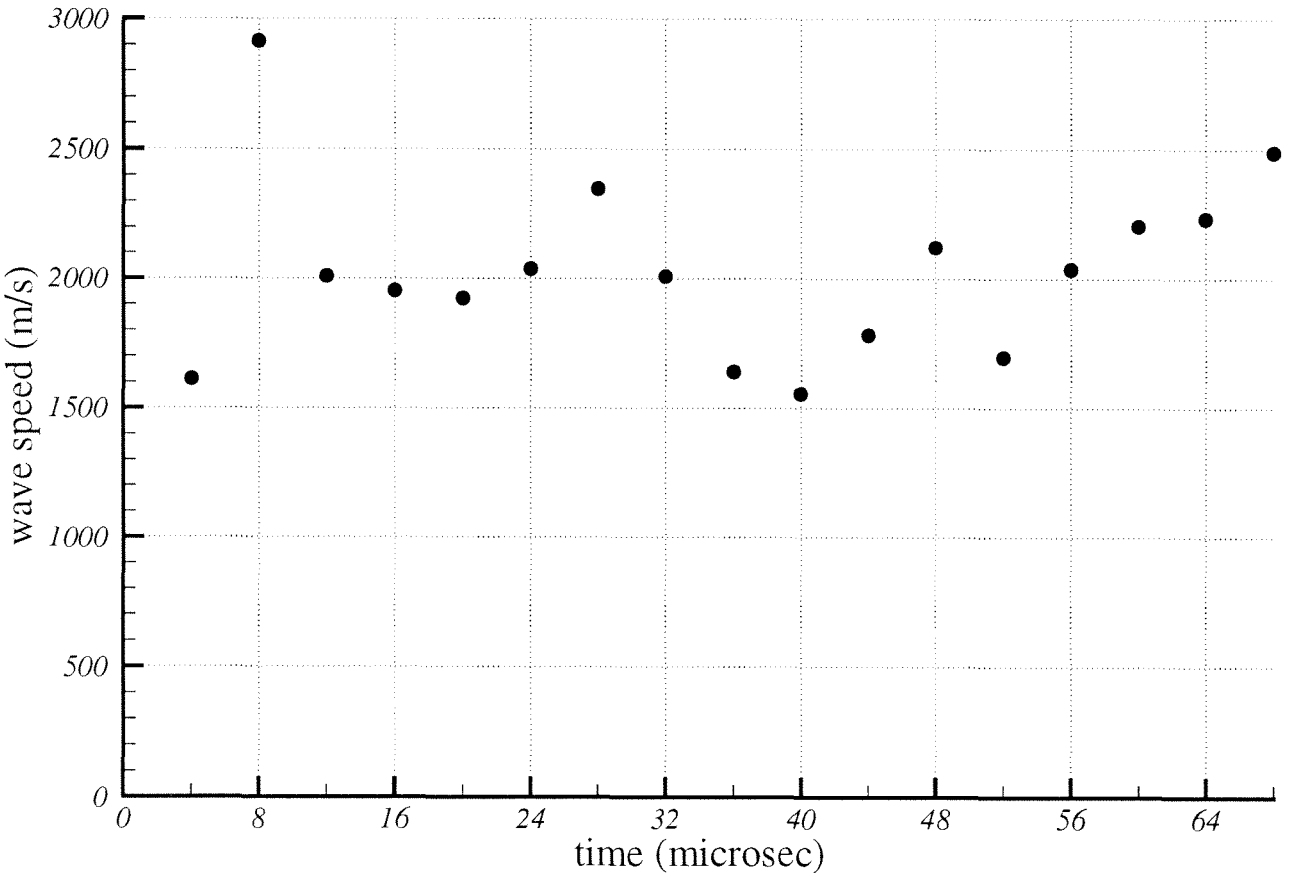

Figure 4.1 : Stress wave speed.

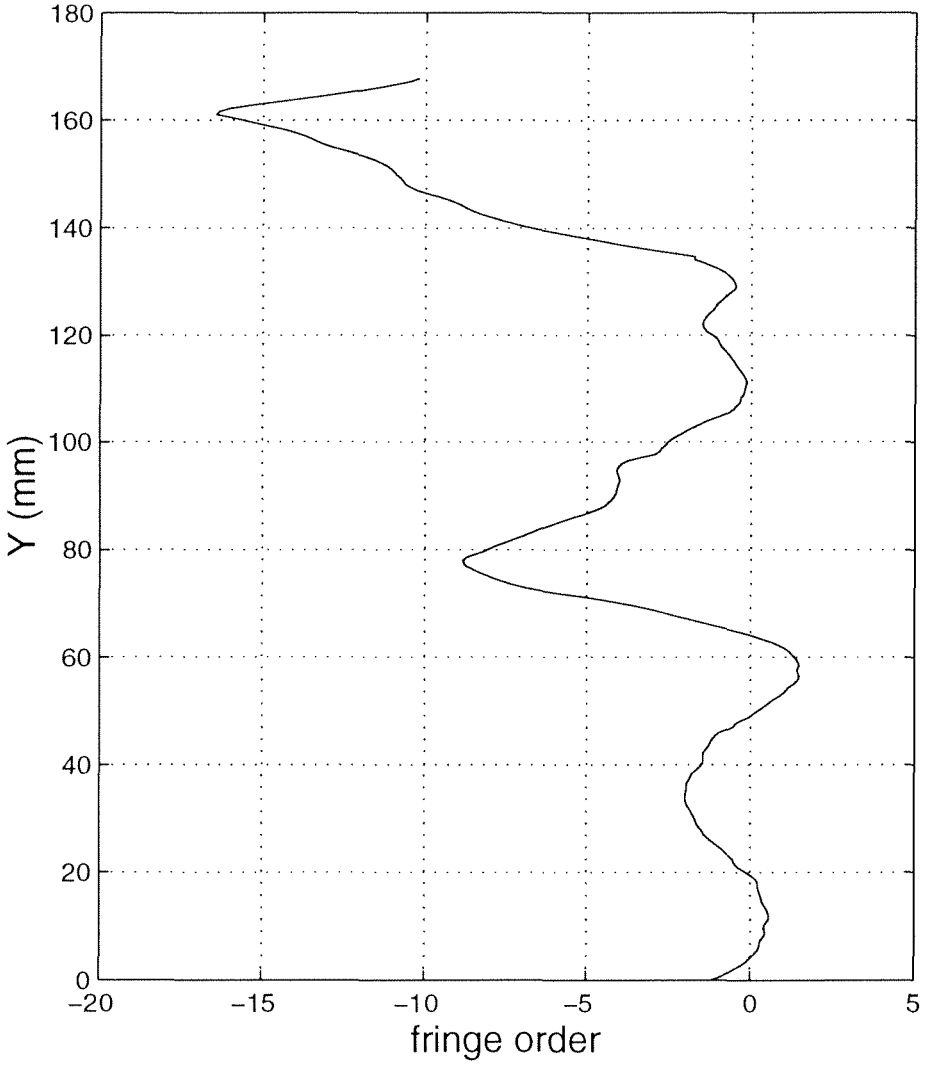

Figure 4.2 : Stress wave profile.

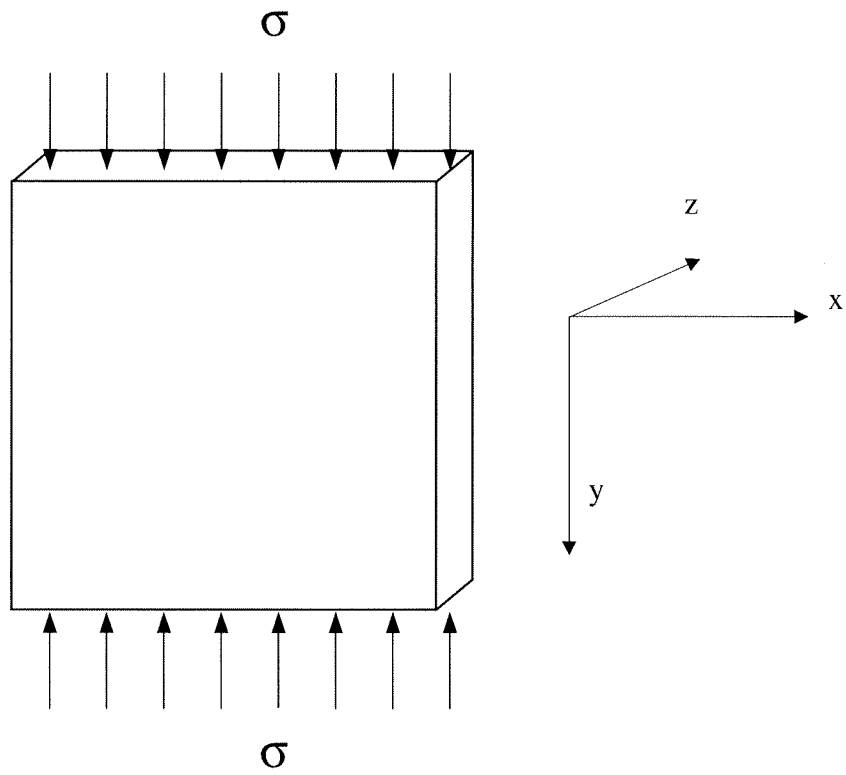

Figure 4.3 : Specimen in uniaxial loading.

5. References

1. Teudt, R., Knauss, W. G., "Studies for Observing Stress Wave Propagation in Polystyrene," *Solid Mechanics Report 93-20, California Institute of Technology, Pasadena, California,* 1993.

2. Teudt, R., Knauss, W. G., "Method for Casting Optically Flat (One Side) Brittle Polystyrene Plates," *Solid Mechanics Report 93-30, California Institute of Technology, Pasadena, California,* 1993.

3. Teudt, R., Knauss, W. G., "Vapor Deposition of Aluminum on Brittle Polystyrene Plates," *Solid Mechanics Report 93-39, California Institute of Technology, Pasadena, California,* 1993.

4. Washabaugh P., "An Experimental Investigation of Mode-I Crack Tip Deformation," *Doctoral Dissertation, California Institute of Technology, Pasadena, California,* 1990.

5. Ravichandar, K., "Personal Correspondence," *Assistant Professor, University of Houston, Houston,* 1997.

6. Ravichandar, K., "An Experimental Investigation into Mechanics of Dynamic Fracture," *Doctoral Dissertation, California Institute of Technology, Pasadena, California,* 1982.

7. Smith, G., "An Experimental Investigation of the Dynamic Fracture of a Brittle Material," *Doctoral Dissertation, California Institute of Technology, Pasadena, California,* 1975.

8. Parthiban, V., Sirohi, R. S., "Interactive Fringe Processing Algorithm for Interferogram Analysis," *Optics and Lasers in Engineering,* Vol. 11, 1989, pp. 103-113.

9. Krishnaswamy, S., "An Algorithm for Computer Tracing of Interference Fringes," *Solid Mechanics Report 89-12, California Institute of Technology, Pasadena, California,* 1989.

10. Born, M., Wolf, E., "Principles of optics : electromagnetic theory of propagation, interference and diffraction of light," *Pergamon Press,* 6th Edition, 1989.

11. Hecht, E., Zajac, A., "Optics," *Addison-Wesley Pub. Co.,* 1974.

12. Jenkins, F. A., White, H. E., "Fundamentals of Optics," *New York, McGraw-Hill Book Company Inc.,* 3rd Edition, 1957.

13. Washabaugh, P., "Personal Correspondence," *Assistant Professor, University of Michigan, Ann-Arbor,* 1996.

APPENDIX

A repeatable procedure has been developed to cast the Break-Away glass material into a 300×300 mm plate specimen of 6 mm thickness and is presented below.

(a) Mold Preparation

(i) Clean the mold and the side bars using acetone and alcohol. Use a brass bar (brass, being softer than steel, does not scratch the mold surface) to remove any material sticking to the surface. Surfaces should be cleaned with alcohol after using acetone, as Break-Away glass is partially soluble in acetone.

(ii) Apply 12 mm wide Teflon tapes to the side bars of the mold and along the edges of the bottom plate of the mold. This reduces stress build-up in the specimen, during cooling.

(iii) Mask a 75×150 mm region at the center of the mold and apply a thin coat of Teflon based mold release agent over the remainder of the surface. The corresponding region in the specimen will later be coated with Aluminum vapor to attain a mirror like finish, and hence contamination with the mold release agent in this area should be avoided.

(iv) Place an $130 \times 130 \times 6$ mm Break-Away glass plate, supplied by the manufacturer, on the mold and bolt the side bars to their respective places. The side bars and the sides of the bottom mold are numbered to ensure high tolerance in dimensions.

(v) Place the mold with the Break-Away glass plate in the oven and close the oven. Note that the top plate of the mold is not used. This is because Break-Away glass

is very brittle and when cooled down it will crack under the weight of the top mold.

(b) Heating

After several preliminary studies, the following procedure was found to be optimal. Heat the mold with Break-Away in it to 140 ^{o}C, let it soak at this temperature for around 15 hours and thus let any trapped air escape. When there are no visible air bubbles inside the material, cool it down to 75 ^{o}C, and loosen the side bars so that the sides of specimen are no longer in contact with the bars. Then cool the mold down very slowly to room temperature. The detail is described below and is programmed in the files of the temperature controller.

File 1:

Step 1 : Set temperature to 128 (123) ^{o}C in 1 hr 30 minutes.

Step 2 : Soak for 3 hrs.

Step 3 : Set temperature to 142 (137) ^{o}C in 1 hr.

Step 4 : Soak for 15 hrs.

Step 5 : Set temperature to 128 (123) ^{o}C in 3 hr.

Step 6 : Go to File 2.

File 2:

Step 1 : Soak for 3 hrs.

Step 2 : Set temperature to 82 (77) ^{o}C in 1 hr.

Step 3 : Hold.

The side bars are loosened at this point so that the sides of specimens do not stick to them. Then file 3 is run.

File 3:

Step 1 : Set temperature to 72 (68) ^{o}C in 1 hr.

Step 2 : Soak for 4 hrs.

Step 3 : Set temperature to 58 (54) ^{o}C in 1 hr.

Step 4 : Soak for 3 hrs.

Step 5 : Set temperature to 49 (46) ^{o}C in 1 hr.

Step 6 : Go to File 4.

File 4:

Step 1 : Soak for 2 hrs.

Step 2 : Set temperature to 38 (36) ^{o}C in 1 hr.

Step 3 : Set temperature to 30 (29) ^{o}C in 1 hr.

Step 4 : End and hold.

The temperature figures are for the upper plate of the oven, and those given in brackets are for the lower plate of the oven.

(c) Aluminum Coating

At room temperature, the specimen is removed carefully from the mold. The flat side of the plate is coated with Aluminum vapor using the available coating facility at GALCIT.